The Atmospherically Important Reaction of Hydroxyl Radicals with Methyl Nitrate: A Theoretical Study Involving the Calculation of Reaction Mechanisms, Enthalpies, Activation Energies, and Rate Coefficients

by

Maggie Ng,[a] Daniel K. W. Mok,[a] Edmond P. F. Lee,*[,a,b] and John M. Dyke*[,b]

a Department of Applied Biology and Chemical Technology, Hong Kong Polytechnic University, Hung Hom, Hong Kong.

b School of Chemistry, University of Southampton, Southampton SO17 1BJ, U.K. emails: epl@soton.ac.uk; jmdyke@soton.ac.uk

Abstract

A theoretical study, involving the calculation of reaction enthalpies and activation energies, mechanisms and rate coefficients, has been made of the reaction of hydroxyl radicals with methyl nitrate, an important process for methyl nitrate removal in the earth's atmosphere.

Four reaction channels were considered:- formation of $H_2O + CH_2ONO_2$, $CH_3OOH + NO_2$, $CH_3OH + NO_3$, and $CH_3O + HNO_3$. For all channels, geometry optimization and frequency calculations were carried out at the M06-2X/6-31+G** level, while relative energies were improved at the UCCSD(T*)-F12/CBS level. The major channel is found to be the H abstraction channel, to give the products $H_2O + CH_2ONO_2$. The reaction enthalpy (ΔH_{298K}^{RX}) of this channel is computed as -17.90 kcal.mol^{-1}. Although the other reaction channels are also exothermic, their reaction barriers are high (> 24 kcal.mol^{-1}) and therefore these reactions do not contribute to the overall rate coefficient in the temperature range considered (200-400 K). Pathways via three transition states have been identified for the H abstraction channel. Rate coefficients were calculated for these pathways at various levels of variational transition state theory (VTST) including tunneling. The results obtained are used to distinguish between two sets of experimental rate coefficients, measured in the temperature range 200-400K, one of which is approximately an order of magnitude greater than the other. This comparison, as well as the temperature dependence of the computed rate coefficients, shows that the lower experimental values are favoured. The implications of the results to atmospheric chemistry are discussed.

Introduction

Alkyl nitrates act as temporary reservoirs of nitrogen oxide radicals in the lower atmosphere as they have relatively long atmospheric lifetimes, of the order of days to weeks (1,2). This enables them to undergo long-range transport to remote areas where they can release NO_x (defined here as $NO + NO_2 + NO_3$) that can give rise to ozone formation. As a result, alkyl nitrates play an important role in contributing to the concentration of O_3 in the troposphere. Methyl nitrate (CH_3ONO_2) and ethyl nitrate ($C_2H_5ONO_2$) are present in the atmosphere mainly from marine emissions (3-6) whereas larger alkyl nitrates are predominantly produced through atmospheric oxidation of hydrocarbons in the presence of NO_x (*e.g.* in urban or polluted areas) (1-7). CH_3ONO_2 and $C_2H_5ONO_2$ account for 20-40% of the light ($C_n \leq 5$) alkyl nitrates in the atmosphere with concentrations of 1-43 pptv and 1-50 pptv respectively having been measured (3,6,8). For the heavier alkyl nitrates, with 4 or more carbon atoms, the association reaction of NO with RO_2 becomes a significant alkyl nitrate source i.e. $RO_2 + NO + M \rightarrow RONO_2 + M$ (M is a third body), whereas for $C_n \leq 4$ the major product channel from the $RO_2 + NO$ reaction is $RO + NO_2$.

A number of recent regional and global model studies have demonstrated that key kinetic and photolytic parameters for alkyl nitrates are missing, preventing chemical models from describing their atmospheric oxidation chemistry adequately and hence obtaining their atmospheric lifetimes (9,10). These parameters include their loss rate via reaction with OH and O_3, and whether NO_x is released in these reactions. Also, how much NO_x (photochemically reactive nitrogen oxide) and how much HNO_3 (photochemically non-reactive nitrogen oxide) are eventually formed from organic nitrate reactions is important in understanding the contribution of alkyl nitrates to the oxidizing capacity of the atmosphere (8). In a recent study of the mechanism of the atmospherically relevant reaction of chlorine atoms with methyl nitrate and calculation of the rate coefficient of this reaction at temperatures relevant to the atmosphere (11), we noted that the lifetime of methyl nitrate in the atmosphere is determined by loss through photolysis, reaction with OH and reaction with Cl atoms. This is because methyl nitrate is thermally stable in the troposphere in the temperature range 200-300 K and heterogeneous removal is slow because its solubility in and reactivity with water is low. The photolysis rate of CH_3ONO_2 in the atmosphere has been determined on a number of occasions (12,13) and the rate coefficient (k) of the $Cl + CH_3ONO_2$ reaction is now reliably known in the temperature

range 200-300 K (11). However, the rate coefficient of the OH + CH_3ONO_2 reaction in this temperature range is not well established. Available experimental rate coefficients at 298 K occur in two groups which differ by an order of magnitude, a lower group at ~$3x10^{-14}$ cm^3 $molecule^{-1}$ s^{-1} (14-17) and a higher group at ~$3x10^{-13}$ cm^3 $molecule^{-1}$ s^{-1} (18,19). There is also uncertainty over the temperature dependence of this rate coefficient. Nielsen et al. (18) report a value of (3.2 ± 0.5) x 10^{-13} cm^3 $molecule^{-1}$ s^{-1} at 298K and a negative temperature dependence of *k* in the region 298-393 K, whereas Shallcross et al. (15) and Talukdar et al. (14) report 298 K values of (2.33 ± 0.14) x 10^{-14} cm^3 $molecule^{-1}$ s^{-1} and (4.7 ± 1.0) x 10^{-14} cm^3 $molecule^{-1}$ s^{-1} respectively and a positive temperature dependence in the region 220-420 K. Also, Talukdar et al. (14) suggest that the OH + CH_3ONO_2 reaction proceeds via H abstraction, based on the fact that the measured rate coefficient was independent of gas composition, the observed trend of rate coefficients as the size of the alkyl group is increased and the large observed primary kinetic isotope effect (as seen in the ratio of the *k*'s measured for OH + CH_3ONO_2 vs OH + CD_3ONO_2). However, the mechanism of the reaction is not well established

In this work, the following reaction channels were considered

H abstraction: $OH + CH_3ONO_2 \rightarrow H_2O + CH_2ONO_2$ ----------(1)

NO_2 formation: $OH + CH_3ONO_2 \rightarrow CH_3OOH + NO_2$ ----------(2)

NO_3 formation: $OH + CH_3ONO_2 \rightarrow CH_3OH + NO_3$ ----------(3)

HNO_3 formation: $OH + CH_3ONO_2 \rightarrow CH_3O + HNO_3$ ----------(4)

Using available heats of formation ($\Delta H_{f,298K}$) of the respective reactants/products, the enthalpies of these reactions, ΔH_{298K}^{RX}, were evaluated as ΔH_1 = -17.72 kcal.mol^{-1}, ΔH_2 = -2.41 kcal.mol^{-1}, ΔH_3 = -9.83 kcal.mol^{-1}, ΔH_4 = -7.22 kcal.mol^{-1} (see Tables 1, 2, 4-7; *vide infra*).

CH_3ONO_2 has a C_s structure with the methyl group staggered with respect to the cis oxygen of the NO_2 group (20). The methyl V_3 rotational barrier is 811 cm^{-1}. In the CH_3 group, one hydrogen atom is in the plane of the heavy atoms, trans to the O-N bond of the C-O-N unit, while the other two hydrogen atoms lie above and below the plane respectively.

The aim of this work is to use state-of-the-art wavefunction and DFT methods to investigate the reaction mechanisms of these OH + CH_3ONO_2 reactions and to compute reaction rate coefficients in the 200-400 K region which should be valuable to test the available experimental values and to decide which experimental values are the more reliable.

Theoretical considerations and computational details

Ab initio and DFT calculations

Geometry optimization, transition state (TS) search, intrinsic reaction coordinate (IRC) and vibrational frequency calculations were carried out using the M06-2X functional (21) and the 6-31+G** basis set with the Gaussian 09 suite of programs (22). The M06-2X functional was chosen because it has been shown to perform particularly well for TS structures and reaction barrier heights in some recent benchmark studies (23-26). In the IRC calculations, using the Hessian-based predictor-corrector (HPC) reaction path following method (27-29), 15 points from the TS in each direction towards the reactants and products were computed with a step size of 0.1 Bohr, and gradients and Hessians were calculated analytically at every IRC point. The computed IRC paths of all the reaction channels cover reaction coordinates of up to *ca.* $s = \pm 1.50$ Bohr.

Electronic energies of the reactants, products, TSs, reactant complexes (RCs) and product complexes (PCs) were improved by performing single-point energy calculations with the explicitly correlated UCCSD(T*)-F12x (where x = a or b) methods (30,31) on the geometries optimized at the M06-2X/6-31+G** level using the MOLPRO suite of programs (32,33). The VTZ-F12 and VQZ-F12 basis sets (34) were employed for the atomic orbital (AO) basis sets. The corresponding AVXZ/MP2FIT (35) basis sets (X = T or Q) were used to compute the F12 integrals by density fitting (DF) while the VXZ-F12/OPTRI (34) basis sets were used to compute the many electron integrals by the resolution of identity (RI) method. The computed UCCSD(T*)-F12x/VTZ-F12 and UCCSD(T*)-F12x/VQZ-F12 relative electronic energies, with respect to the separate reactants, were extrapolated to the complete basis set (CBS) limit employing two schemes. In the first scheme, the two-point $1/X^3$ formula of Helgaker et al. (36,37) was used to extrapolate the relative electronic energies computed at the UCCSD(T*)-F12x/VTZ-F12 and UCCSD(T*)-F12x/VQZ-F12 levels, and the extrapolated relative electronic energies are denoted as CBS1. In the other scheme, the relative electronic energies computed at the UCCSD(T*)-F12x/VTZ-F12 and UCCSD(T*)-F12x/VQZ-F12 levels were extrapolated to the CBS limit by the generalized formula of Schwenke (38), with the CBS coefficients optimized by Hill et al. (39) for CCSD-F12b energies with the VTZ-F12/VQZ-F12 basis set combination. The extrapolated relative electronic energies thus obtained are denoted as CBS2. The averages of the computed UCCSD(T*)-F12a/CBS1//M06-2X/6-31+G**, UCCSD(T*)-F12b/CBS1//M06-2X/6-31+G**, UCCSD(T*)-F12a/CBS2//M06-2X/6-31+G** and UCCSD(T*)-F12b/CBS2//M06-2X/6-31+G** relative electronic energies, labelled as UCCSD(T*)-F12ave/CBSave//M06-2X, are considered to be the best theoretical estimates in the present study. The choice of the average value as the best theoretical estimate is mainly because the values obtained by the various extrapolation schemes described above are very

close to each other (vide infra).

In the $^2\Pi$ state of OH, the spin-orbit (SO) splitting of 139.6 cm^{-1} results in an energy lowering of the unperturbed $^2\Pi$ state to the $^2\Pi_{3/2}$ state of 0.20 kcal mol^{-1} (40). Therefore, all the computed relative energies, namely, reaction enthalpies (ΔH_{298K}^{RX}), reaction energies (ΔE^{RX}) and activation energies ($\Delta E^{\ddagger}$), were increased by 0.20 kcal mol^{-1} to allow for this. This correction has also been applied to the relative energy of the RCs and PCs, notably for reaction 1. Also, the electronic partition functions of both the $^2\Pi_{3/2}$ and $^2\Pi_{1/2}$ states of OH, together with the appropriate energies and degeneracies, were included in the subsequent rate coefficient calculations.

For reactions (1)-(4), the transition states that were located in the M06-2X calculations can be summarised as follows (*vide infra)*:-

H abstraction: $OH + CH_3ONO_2 \rightarrow TS_{1a} / TS_{1b} / TS_{1c} \rightarrow H_2O + CH_2ONO_2$ ----(1′)

NO_2 formation: $OH + CH_3ONO_2 \rightarrow TS_2 \rightarrow CH_3OOH + NO_2$ ----(2′)

NO_3 formation: $OH + CH_3ONO_2 \rightarrow TS_3 \rightarrow CH_3OH + NO_3$ ----(3′)

HNO_3 formation: $OH + CH_3ONO_2 \rightarrow TS_{4a} \rightarrow CH_3O + HNO_3$ ----(4′)

$OH + CH_3ONO_2 \rightarrow TS_{4b} \rightarrow CH_3O(OH)NO_2$ conformer 1

$\rightarrow TS_{rot} \rightarrow CH_3O(OH)NO_2$ conformer 2 $\rightarrow TS_{4c} \rightarrow CH_3O + HNO_3$

Rate coefficient calculations

Reaction rate coefficients were computed for the H abstraction channel {channel (1)} at various TST levels in single-level and improved single-level direct dynamics calculations at temperatures in the region 200-400 K using the POLYRATE 2010-A program (41). The rate coefficients obtained correspond to rate coefficients obtained in the high pressure limit. As the computed barrier heights of channels (2), (3) and (4) are considerably higher than that of channel (1), only channel (1) was considered in the rate coefficient calculations. In addition, for channel (1), the computed energies of TS_{1b} and TS_{1c} relative to the reactants are higher than that of TS_{1a} by *ca.* 2-3 kcal mol^{-1} and therefore it is expected that TS_{1a} would contribute the most to the total rate coefficient of channel (1).

The geometries of the reactants, reactant complex (RC), TS, product complex (PC), products and the 30 non-stationary points on the IRC path obtained at the M06-2X/6-31+G** level, together with the corresponding analytical gradients and Hessians, were used in the single-level direct dynamics calculations. All the methyl torsional modes (in CH_3ONO_2 and the

RC) were treated as hindered internal rotations within the hindered-internal-rotator (HIR) approximation (42) using the full Chuang-Truhlar (CT) method (43,44). The V_{MEP} curves were obtained by interpolation/extrapolation in the range of s = ±0.86 Å using the Euler-steepest-descents (ESD) method (45) with a Hessian step size of 2.39 x 10^{-3} Å, which is nine times larger than the gradient step size of 2.65 x 10^{-4} Å. In the generalized normal mode analysis, curvilinear internal coordinates (46) were used instead of the redundant internal coordinates (47) because it was found in the present study that the redundant internal coordinates gave extra imaginary vibrational frequencies, which indicate unphysical descriptions of the vibrational motions of the molecules. With curvilinear internal coordinates, no extra imaginary vibrational frequency was found along the minimum energy path (MEP). Rate coefficients were calculated at different TST levels, namely, conventional transition state theory (TST), canonical variational transition state theory (CVT) and improved canonical variational transition state theory (ICVT), with different tunneling methods, including zero-curvature tunneling (ZCT) and small-curvature tunneling (SCT) corrections.

Improved single-level direct dynamics calculations (48) were carried out, with the M06-2X/6-31+G** V_{MEP} curve as the lower level (LL) and the higher-level (HL) V_{MEP} curve obtained by using the computed HL energies of five stationary points, namely, the separated reactants, RC, TS, PC and the separated products computed at the UCCSD(T*)-F12ave/CBSave level (the average of the four CBS values). More IRC points on the HL V_{MEP} were obtained by the following scaling expression devised by us previously (equation (5),(49)).

$$E_s^{HL} = (E_s^{LL} - E_{RC}^{LL}) \times \{(E_{TS}^{HL} - E_{RC}^{HL})/(E_{TS}^{LL} - E_{RC}^{LL})\} + E_{RC}^{HL} \quad \text{---------- (5)}$$

With this expression, an improved HL energy (E_s^{HL}) at a certain s along the LL IRC can be evaluated using the LL energy (E_s^{LL}) and the ratio between the computed HL and LL barriers. Together with the HL energies of the five stationary points, the additional HL IRC energies obtained from this scaling expression were used in improved single-level rate coefficient calculations with the geometries and vibrational frequencies at the lower level. This scaling formula gave almost identical rate coefficients as those obtained with the dual-level mapping method of POLYRATE (48) (more detail is given in the Supplementary Information section SI1).

Results and discussion

Ab initio and DFT results

From the results of the *ab initio* and DFT calculations, channels (2), (3) and (4) were

found to have considerably higher barrier heights (> 20 kcal mol^{-1}) than channel (1). As a result, channel (1) is the dominant pathway of the OH + CH_3ONO_2 reaction and will be considered, after channels (2), (3) and (4) have been discussed. The contributions of channels (2), (3) and (4) to the total rate coefficient of the OH + CH_3ONO_2 reaction are expected to be negligibly small and hence they were neglected in the subsequent rate coefficient calculations.

Inspection of the results of UCCSD(T*)-F12x calculations shows that the effects of basis set size on the computed ΔE_e^{RX} and $\Delta E_e^{\ddagger}$ (the reaction energy and activation energy respectively calculated using only electronic energies), the energy differences between the F12a and F12b results, and those between the two CBS extrapolation schemes (CBS1 and CBS2) are small in all channels, as the energy differences are within chemical accuracy (1 kcal. mol^{-1}). The geometries of the TSs in all channels, optimized at the M06-2X/6-31+G** level, are shown in Figure 1, while those of the adduct conformers in channel (4) and those of the RC and PC in channel (1) are shown in Figure 2. Furthermore, the ΔE_{0K} values computed at the UCCSD(T*)-F12ave/CBSave//M06-2X level are summarized in the energy profile in Figure 3.

NO_2 formation: OH + CH_3ONO_2 → CH_3OOH + NO_2 --- Channel (2)

The geometry of the TS in channel (2′), TS_2, optimized at the M06-2X/6-31+G** level is shown in Figure 1. The computed imaginary vibrational frequency of TS_2, 988i cm^{-1}, corresponds to the asymmetric O…O…N stretching mode, indicating that TS_2 undergoes O-N bond breaking and O-O bond formation via a S_N2 mechanism to release NO_2, when the O atom of the OH radical attacks the O atom next to the methyl group. In TS_2, the breaking C-N bond is elongated by 33% while the forming O-O bond is longer than that in CH_3OOH by 22%. Hence, it is not obvious whether TS_2 is reactant-like or product-like, as the elongations of the breaking C-N bond and the forming O-O bond are comparable. The computed reaction energies (ΔE_e^{RX}) and activation energies ($\Delta E_e^{\ddagger}$) of channel (2) at various levels of theory are summarized in Table 1. The best computed ΔE_e^{RX} and $\Delta E_e^{\ddagger}$ values (labelled as F12ave/CBSave) are -1.72 ± 0.01 and 24.08 ± 0.17 kcal mol^{-1}. Including the zero-point energy (ZPE) correction and the spin-orbit correction for OH, the best computed ΔE_{0K}^{RX} and $\Delta E_{0K}^{\ddagger}$ values of -1.21 and 24.56 kcal mol^{-1} are obtained. This indicates that channel (2) has a high activation barrier and, therefore, its contribution to the total rate coefficient of the OH + CH_3ONO_2 reaction is negligible (more detail is given in the Supplementary Information section SI2).

NO_3 formation: OH + CH_3ONO_2 → CH_3OH + NO_3 --- Channel (3)

The geometry of the TS in channel (3′), TS_3, optimized at the M06-2X/6-31+G** level is shown in Figure 1. The imaginary vibrational frequency of 1251i cm^{-1} corresponds to the asymmetric O…C…O stretching mode, which shows that TS_3 undergoes O-C bond breaking and C-O bond forming via a S_N2 mechanism to release NO_3 when the O atom in the OH radical attacks the C atom in the methyl group. The breaking O-C bond in TS_3 is elongated by 29% while the forming C-O bond is longer than the equilibrium value of 1.41 Å in CH_3OH by 25%, and so the TS_3 is not reactant-like or product-like. The computed ΔE_e^{RX} and $\Delta E_e^{\ddagger}$ values at various levels of theory are summarized in Table 2. The best computed ΔE_e^{RX} and $\Delta E_e^{\ddagger}$ values at the F12ave/CBSave level are -7.99 ± 0.12 and 36.07 ± 0.11 kcal mol^{-1} respectively, and the corresponding best computed ΔE_{0K}^{RX} and $\Delta E_{0K}^{\ddagger}$ values are -7.73 and 37.09 kcal mol^{-1}. Although the computed ΔH_{298K}^{RX} value of -8.01 kcal mol^{-1} indicates that channel (3) is exothermic, the large reaction barrier height of 37.09 kcal mol^{-1} means that this reaction will only make an extremely small contribution to the overall OH + CH_3ONO_2 rate coefficient. As a result, channel (3) was also not considered in the rate coefficient calculations (more detail is given in the Supplementary Information section SI3).

HNO_3 formation: OH + CH_3ONO_2 → CH_3O + HNO_3 --- Channel (4)

The reaction leading to HNO_3 formation can take place through a concerted mechanism, in which the reactants proceed to the products via a transition state, or through a stepwise mechanism involving adduct formation (see equation 4′). Both pathways are calculated to have high activation energies (> 28 kcal.mol^{-1}) and therefore this channel is not expected to contribute to the overall reaction rate coefficient (more detail is given in the Supplementary Information section SI4).

H abstraction: OH + CH_3ONO_2 → H_2O + CH_2ONO_2 --- Channel (1)

In channel (1), a H atom of the methyl group of CH_3ONO_2 is abstracted by the OH radical to give H_2O and CH_2ONO_2. As shown in equation (1′), three TS's have been located and their optimized geometries at the M06-2X/6-31+G** level are shown in Figure 1. Some major geometrical parameters, the imaginary vibrational frequencies, the ΔE_e and ΔE_{0K} values as well as the ZPE corrections of the three TS's are summarized in Table 6. In TS_{1a} and TS_{1b}, the OH radical abstracts the out-of-plane H atom, with the O-H bond in the OH radical nearly parallel to the C_s plane of CH_3ONO_2. The geometry of TS_{1a} is similar to that of TS_{1b}, except that in TS_{1a} the H atom in the OH radical points towards the O atom in the nitrate group and

this results in a O---H hydrogen bond-like interaction with a distance of 2.34 Å between the O and H atoms. In TS_{1c}, the OH radical abstracting the in-plane H atom is in the C_s plane of CH_3ONO_2, and the O-H bond in the OH radical is almost parallel to the C-O bond. TS_{1a}, TS_{1b} and TS_{1c} have imaginary vibrational frequencies of 1294i, 1135i and 1486i cm^{-1} respectively (see Table 6), which correspond to the asymmetric C···H···O stretching mode. The *L* parameters determined from the ratio of the elongation of the breaking C-H bond to that of the forming H-O bond {$L = \Delta(C\text{-}H)/\Delta(H\text{-}O)$} are 0.39, 0.25 and 0.39 for TS_{1a}, TS_{1b} and TS_{1c} respectively, indicating that all the three TS's are reactant-like because their *L* parameters are smaller than 1. It can be seen that both the ΔE_e and the ΔE_{0K} values of the TS's are in the order $TS_{1c} > TS_{1b} > TS_{1a}$. TS_{1a} has the lowest energy of the three TS's, as expected, due to the presence of the hydrogen bond-like interaction, which stabilizes TS_{1a} by *ca*. 1.5 to 2 kcal mol^{-1}. The best computed activation energies (ΔE_e without ZPE and OH spin-orbit corrections) to the transition states TS_{1a}, TS_{1b} and TS_{1c}, at the F12ave/CBSave level, are 4.02, 5.52 and 7.05 kcal mol^{-1} respectively. They are within 1 kcal.mol^{-1} of the corresponding M06-2X values (3.01, 5.10 and 6.23 kcal.mol^{-1}), suggesting that the M06-2X functional performs well for barrier heights of this channel, especially for TS_{1b} where the energy difference between the M06-2X and the F12ave/CBSave levels is 0.42 kcal mol^{-1}. With the ZPE and spin-orbit corrections, the best computed activation energies (ΔE_{0K}) associated with TS_{1a}, TS_{1b} and TS_{1c} are 2.76, 4.02 and 5.04 kcal mol^{-1} respectively, showing that channel (1) has the lowest barrier height of all channels and hence is the dominant pathway of the OH + CH_3ONO_2 reaction. This supports the conclusion of the study of Talukdar *et al.* (14) that the OH + alkyl nitrate reaction proceeds via simple H abstraction, rather than OH addition suggested by He *et al*. (8).

Regarding the out-of-plane OH + $CH_3ONO_2 \rightarrow H_2O + CH_2ONO_2$ channel via TS_{1a}, a RC and a PC (labelled as RC_{1a} and PC_{1a} respectively) have been located in the entrance and exit channels respectively. The geometries of the RC_{1a} and PC_{1a} optimized at the M06-2X/6-31+G** level are shown in Figure 2. In the seven-membered ring RC_{1a}, there is an interaction between the H atom of the OH radical and the O atom in the nitrate group with a O---H distance of 2.51 Å. In PC_{1a}, the two H atoms in H_2O are oriented to enable interactions with the two O atoms in the nitrate group with O---H distances of 2.96 Å and 3.25 Å. The computed ΔE_e, ΔE_{0K} and ΔH_{298K} values of the RC_{1a} and PC_{1a}, together with those of TS_{1a} and the separate products, obtained at various UCCSD(T*)-F12x//M06-2X/6-31+G** levels are summarized in Table 7. These values were used in the rate coefficient calculations with POLYRATE. The energies of the RC_{1a} and PC_{1a} are lower than the separate reactants and products, respectively, by *ca*. 3 kcal

mol^{-1}. The best computed ΔE_e values of the RC_{1a}, TS_{1a}, PC_{1a} and the separate products at the F12ave/CBSave level are -3.01 ± 0.01, 4.02 ± 0.05, -20.51 ± 0.07 and -17.23 ± 0.08 kcal mol^{-1} respectively. The estimated uncertainties are within 0.1 kcal mol^{-1}, which are negligibly small, for all the species. It was found that the M06-2X functional performs reasonably well for the ΔE_e values of TS_{1a} and PC_{1a}, and fairly well for the ΔE_e values of RC_{1a} and the separate products, as the differences between the M06-2X and the F12ave/CBSave values for RC_{1a}, TS_{1a}, PC_{1a} and separate products are 2.41, 1.03, 0.20 and 2.64 kcal mol^{-1} respectively. The best computed ΔH_{298K}^{RX} value (including the spin-orbit correction) for channel (1) is -17.90 kcal mol^{-1}, which is lower than the ΔH_{298K}^{RX} of -13.92 kcal mol^{-1} evaluated from the available $\Delta H_{f,298K}$ values of CH_3ONO_2 (50), OH (51), CH_2ONO_2 (50), and H_2O (52) by *ca*. 4 kcal mol^{-1}. However, it agrees very well with the ΔH_{298K}^{RX} value of -17.72 kcal mol^{-1} determined using these $\Delta H_{f,298K}$ values but with the $\Delta H_{f,298K}$ values for CH_3ONO_2 and CH_2ONO_2, obtained from the tabulation of Burcat et al. (50), replaced by -29.71 and 19.30 kcal mol^{-1} respectively, computed in our previous study (11).

Rate coefficients of the OH + CH_3ONO_2 → H_2O + CH_2ONO_2 channel

Computed rate coefficients at the M06-2X single level

The reaction paths, including the V_{MEP}, ΔZPE and V_a^G curves, obtained at the M06-2X/6-31+G** level for the OH + CH_3ONO_2 → H_2O + CH_2ONO_2 C-H out-of-plane channel via TS_{1a} are shown in Figure 4 (upper panel). There is a dip of ~ 3 kcal mol^{-1} in the ΔZPE curve near the saddle point region (s = 0), which leads to a shift of the maximum of the V_a^G curve to s = -0.16 Å. The computed rate coefficients for this channel (k_{1a}), obtained at different VTST levels using the M06-2X IRC, plotted against temperature are shown in Figure 5. The available experimental values (14-19) determined in the temperature range of 200-423 K are also included in the lower part of this figure ($\log_{10}k$ vs 1000/T). It should be noted that all the computed rate coefficients (k_{1a}) have been multiplied by two to account for the two possible C-H out-of-plane H abstraction sites. The higher sets of experimental values from Nielsen et al. (18) and Kerr et al. (19) are not shown in the upper part of Figure 5, the k vs T plot, as they are considerably larger than the other values and out of the k scale of the plot. As expected, the computed TST rate coefficients, k^{TST}, at a given temperature are larger than all the VTST computed values. They are larger than the CVT and ICVT values by an order of magnitude, indicating that the variational effect is significant. The tunneling effects, whether with ZCT or SCT, are small when T > 360 K, as the transmission coefficients are close to unity. However,

the tunneling effects become more significant as temperature decreases. The transmission coefficients with ZCT and SCT at 200 K are 4.56 and 9.64 respectively; thus the SCT correction at this temperature can increase the computed rate coefficients by nearly an order of magnitude. The classical adiabatic ground-state (CAG) correction (53-55) accounts for the fact that the generalized transition state (GTS) at the CVT level is not located at the maximum of the V_a^G curve. The CAG factor at the CVT level ($\kappa^{CVT/CAG}$) is close to unity in the range 200-400 K, indicating that the CAG correction with CVT is insignificant, because the maximum of the ΔG curve is located at $s \approx$ -0.15 Å, which is near to the maximum of the V_a^G curve (s = -0.16 Å). Considering the computed rate coefficients at the highest ICVT/SCT level ($k^{ICVT/SCT}$), they are closer to the lower sets of experimental values of Gaffney et al. (16), Talukdar et al. (14), Kakesu et al. (17) and Shallcross et al. (15), than the higher values of Nielsen et al. (18) and Kerr et al. (19), but are lower than the lower group of experimental values by an order of magnitude. In addition, the computed $k^{ICVT/SCT}$ values show a positive temperature dependence which is observed in the lower set of experimental values but not in the higher group, indicating that the computed $k^{ICVT/SCT}$ values, derived from the computed M06-2X reaction paths, favour the lower set of experimental values.

Computed rate coefficients at the UCCSD(T*)-F12ave/CBSave//M06-2X/6-31+G dual level**

The V_{MEP}, ΔZPE and V_a^G curves obtained at the UCCSD(T*)-F12ave/CBSave//M06-2X/6-31+G** level for the OH + CH_3ONO_2 → H_2O + CH_2ONO_2 C-H out-of-plane channel via TS_{1a} are shown in Figure 4 (lower panel). As shown in Table 7, $\Delta E_e^{\ddagger}$ obtained at the UCCSD(T*)-F12ave/CBSave//M06-2X/6-31+G** level is 4.02 kcal.mol^{-1} compared with 3.01 kcal.mol^{-1} at the M06-2X/6-31+G** level (both values are without correction for OH spin-orbit splitting which would increase them both by 0.20 kcal.mol^{-1}).The HL V_{MEP} and V_a^G curves are shown in the lower half of Figure 4. These were obtained using HL energies of the reactants, RC_{1a}, TS_{1a}, PC_{1a} and products, as well as extra HL IRC points calculated by the expression devised by us previously (equation (5) and ref.(49)). The HL F12ave/CBSave V_{MEP} curve follows the shape of the M06-2X V_{MEP} curve and has a maximum of 4.22 kcal mol^{-1} at s = 0. The plots of the rate coefficients computed at various VTST levels for this channel (1(a)) with the HL F12ave/CBSave//M06-2X/6-31+G** IRC in the temperature range between 200 K and 400 K are shown in Figure 6. The spread and the order of the F12ave/CBSave k values at different VTST levels are similar to those of the M06-2X k values. However, the F12ave/CBSave k values are smaller than the corresponding M06-2X values by an order of

magnitude, as the F12ave/CBSave $\Delta E^{\ddagger}$ is higher than the M06-2X $\Delta E^{\ddagger}$ by *ca*. 1 kcal mol^{-1}. Computed ICVT/SCT rate coefficients of reactions (1a), (1b) and (1c) in the temperature range between 200 K and 400 K, as well as the total rate coefficients of the hydrogen atom abstraction reaction, obtained with the HL F12ave/CBSave//M06-2X/6-31+G** IRC, are shown in Figure 7 (see also Tables SI5 and SI6 in the Supplementary Information (SI)). The total rate coefficient has been obtained from $k_{total} = 2k_{1a} + 2k_{1b} + k_{1c}$, as there are two hydrogen atoms in CH_3ONO_2 that could be removed in channels 1a and 1b (the out-of-plane H atoms), but only one that could be removed in channel 1c (the in-plane H atom). This figure shows that k_{1a} is the main contribution to the overall rate coefficient in the temperature range 200-300K, with k_{1b} also becoming significant above 300 K. k_{1c} is significantly lower than k_{1a} by at least an order of magnitude at all temperatures considered, and hence its contribution to k(total) is very small. As can be seen from Figure 7, k_{1b} becomes comparable with k_{1a} at temperatures higher than 280 K, and k_{1b} becomes higher than k_{1a} at temperatures greater than 334K ($1000/T = 2.99$ K^{-1}) . This is somewhat surprising as channel 1b has a higher barrier than channel 1a ($\Delta E_e^{\ddagger}$ values 4.22 (1a) and 5.72 (1b) kcal.mol^{-1} respectively). This arises because the entropy term ($\Delta S^{\ddagger}$) in the rate coefficient ($\Delta S^{\ddagger}$ is negative in both cases) makes a larger contribution to k_{1b} than k_{1a} in the temperature range 340-400 K, such that $\Delta G^{\ddagger}$ is more positive for channel 1a than 1b in the temperature range 340-400 K, whereas $\Delta G^{\ddagger}$ is less positive for channel 1a than 1b in the temperature range 200-340 K

The computed $k^{ICVT/SCT}$ values of channel 1 ($k_{total} = 2k_{1a} + 2k_{1b} + k_{1c}$) at the F12ave/CBSave level fall below the experimental values, indicating that the F12ave/CBSave $\Delta E_e^{\ddagger}$ for TS_{1a} of 4.22 kcal mol^{-1} and $\Delta E_e^{\ddagger}$ for TS_{1b} of 5.72 kcal mol^{-1} (with spin-orbit correction of OH) are too high (see Table 8; the $k^{ICVT/SCT}$ values are shown in column 3). In order to obtain an improved match between theory and experiment, calculations were carried out with reduced barrier heights for channels 1(a), 1(b) and 1(c). A reduction of the barrier heights of channels 1(a), 1(b) and 1(c) of 2.5 kcal mol^{-1} has been made, to give $\Delta E_e^{\ddagger}$ values of 1.72, 3.22 and 4.75 kcal mol^{-1} for these channels, and rate coefficient calculations were carried out with the corresponding HL F12ave/CBSave IRC. This lowering of 2.5 kcal.mol^{-1} in the $\Delta E_e^{\ddagger}$ values made for channels 1(a), 1(b) and 1(c) is similar to the downward correction we had to make in related studies of the Cl + $CH_3C(O)OCH_3$ (49) and Cl + HCOOH (56) reactions of 2.2 and 2.7 kcal.mol^{-1} respectively. k_{total} ICVT/SCT values obtained at different temperatures with this correction are shown in column 2 of Table 8. As can be seen from this table, the experimental rate coefficients fall into two groups. A lower set, where the experimental values of Talukdar

(14) and Shallcross (15) show a positive temperature dependence in the temperature range 220-420 K, and a higher group, where the experimental values of Nielsen (18) show a negative temperature dependence in the temperature range 298-393 K. At 300 K, the computed $k^{ICVT/SCT}$ value with the HL F12ave/CBSave IRC is ~ 30 times lower than the 300 K values of Talukdar (14) and Shallcross (15). However, a 2.5 kcal.mol^{-1} reduction of the $\Delta E_e^{\ddagger}$ values for channels 1(a), 1(b) and 1(c) increases the 300 K $k^{ICVT/SCT}$ value, to give good agreemnt with the 300 K values of Talukdar (14) and Shallcross (15). These computed $k^{ICVT/SCT}$ values also show a positive temperature dependence, as observed in the work of Talukdar and Shallcross (see Figure 8). To increase the computed $k^{ICVT/SCT}$ 300 K value to agree with the higher value of Nielsen (18), requires a reduction in barrier heights $\Delta E_e^{\ddagger}$ of at least 3.5 kcal.mol^{-1}. With such a reduction a positive temperature dependence of $k^{ICVT/SCT}$ is still computed, not a negative temperaure dependence as observed by Nielsen (18). Also, a reduction of $\Delta E_e^{\ddagger}$ of 3.5 kcal.mol^{-1} is larger than we have had to apply to calculations at the same level on related reactions (49,56) to give acceptable agreement with experimental values. Therefore, considering all the evidence it is concluded that the lower set of experimental rate coefficients, with a positive temperature dependence, are to be preferred.

Atmospheric Implications

Both the M06-2X/6-31+G** single level and UCCSD(T*)F12ave/CBSave//M06-2X/6-31+G** improved single level electronic structure / rate coefficient calculations performed in this work favour the lower set of experimental rate coefficients (14-17) over the higher group (18,19). They also support the positive temperature dependence of the rate coefficient in the temperature range 200-400 K observed in the work of refs (14) and (15) rather than the negative temperature dependence observed in ref.(18).

It is valuable to compare the results of this present work on the OH + CH_3ONO_2 reaction with those obtained in our earlier work on the Cl + CH_3ONO_2 reaction (11). Both proceed via a hydrogen abstraction reaction. For the Cl + CH_3ONO_2 reaction, the recommended values for the reaction barrier ($\Delta E_e^{\ddagger}$) and reaction enthalpy (ΔH_{298K}^{RX}) are 0.17 and -2.30 kcal.mol^{-1}, values obtained at the UCCSD(T*)-F12/CBS//M06-2X/6-31+G** level, whereas the corresponding recommended values in this work for the OH + CH_3ONO_2 case are 1.72 (1a) and -17.72 kcal.mol^{-1}. The reaction barrier ($\Delta E_e^{\ddagger}$) is lower in the Cl + CH_3ONO_2 case than in the OH + CH_3ONO_2 reaction, and the Cl+ CH_3ONO_2 rate coefficients are higher, in the temperature range 200-400 K. The Cl + CH_3ONO_2 reaction rate coefficient shows a positive

temperature dependence as is now established for the OH + CH_3ONO_2 case. For the OH + CH_3ONO_2 reaction, as shown in Figure 1, TS_{1a} has a structure with a hydrogen bond between the O of the O-H and an H of the CH_3 group, and a longer hydrogen bond between the H of the O-H and an O of the $-NO_2$ group. In the Cl + CH_3ONO_2 case, this hydrogen bonding is obviously not possible and the transition state structure is similar to that shown for TS_{1b} and TS_{1c} in Figure 1.

As was noted in the Introduction, the lifetime of methyl nitrate in the atmosphere is controlled by photolysis, reaction with Cl atoms and reaction with OH. The photolysis lifetime of methyl nitrate in the troposphere (0-15 km above ground level) has been determined to be in the region of 1-5 days (1,12,13). In the troposphere the temperature typically drops from 288 K at ground level to 216 K at 15 km, and hence the rate coefficients shown in Table 8 in the temperature range 200-300 K are the most relevant to the lower atmosphere. In our earlier work on Cl + CH_3ONO_2 (11), we calculated that for [Cl] = 10^3 atom.cm^{-3}, the estimated day-time global average in the marine boundary layer (57), the methyl nitrate lifetime with respect to this reaction is 3.68×10^4 days at 300 K and 2.49×10^5 days at 200 K, using the now well established Cl + CH_3ONO_2 rate coefficients (11). For the OH + CH_3ONO_2 reaction, the work of Talukdar et al. (14) is the only study in which rate coefficients have been measured in the range 200-300 K. The 298 K rate coefficient of ref.(14) is in the lower group. Also, the rate coefficients determined by these authors in the higher temperature region 300-423 K agree reasonably well with previously determined values in this temperature range by Shallcross et al. (15). The experimental rate coefficients of Talukdar et al. (14) were therefore assumed as a reliable reference for the purposes of calculating the lifetime of methyl nitrate with respect to reaction with OH. This can be calculated at a particular temperature as $1/(k_{OH}$ [OH]), if [OH] and k_{OH} , the OH + CH_3ONO_2 rate coefficient, are known at that temperature. Using OH = 1×10^6 molecule.cm^{-3}, the estimated average day-time concentration of OH (58), with the rate coefficients from Talukdar et al. (14) (see Table 8), the methyl nitrate lifetime with respect to reaction with OH is calculated as 422 (300K) and 2320 (200K) days respectively. Therefore, under normal atmospheric conditions the methyl nitrate lifetimes are in the order

$$\text{Photolysis} < \text{OH}_{\text{reaction}} < \text{Cl}_{\text{reaction}}$$

Concluding remarks

The reaction mechanism of the OH + CH_3ONO_3 reaction has been investigated by

carrying out *ab initio*/DFT calculations on four possible reaction channels:- hydrogen atom abstraction, NO_2 production, NO_3 production and HNO_3 production. All reaction channels are exothermic but the H abstraction channel has a much lower activation energy compared with the other channels. This means that the H abstraction channel will have the highest rate coefficients and is therefore kinetically the most important while NO_2, NO_3 and HNO_3 formation will be minor. The H abstraction channel was found to proceed via three possible pathways involving transition states TS_{1a}, TS_{1b} and TS_{1c} (see Figure 1-3). The pathway via TS_{1a}, a hydrogen bonded transition state, has the lowest activation energy.

ICVT/SCT rate coefficients obtained with the UCCSD(T*)-F12ave/CBSave//M06-2X IRC for the H abstraction reaction (reaction 1) via the three transition states, TS_{1a}, TS_{1b} and TS_{1c}, show that k_{1a} and k_{1b} are the main contributors to the overall rate coefficient ($k_{total} = 2k_{1a} + 2k_{1b} + k_{1c}$) in the temperature range 200-400 K. k_{1c} makes a negligible contribution. k_{1a} is greater than k_{1b} in the atmospherically important temperature range 200-300K with k_{1b} becoming greater than k_{1c} at $T > 334$ K. A reduction in the barrier heights ($\Delta E_e^{\ddagger}$) of TS_{1a} , TS_{1b} and TS_{1c} by 2.5 kcal.mol^{-1} brings the computed k_{total} values in reasonably good agreement with the experimental values over the range 200-400 K. k_{1a}, k_{1b} and k_{1c} all increase with increasing temperature. This behaviour as well as the fact that the k_{total} is less than the lower group of experimental rate coefficients favours the lower experimental rate coefficients over the higher group. The relative importance of the methyl nitrate loss processes (photolysis, reaction with OH and reaction with Cl atoms) in the atmosphere is discussed and the methyl nitrate lifetimes with respect to these processes is shown to be in the order

$$\text{Photolysis} < OH_{reaction} < Cl_{reaction} .$$

In summary, the rate coefficients computed at the highest level favour the lower set of experimental rate coefficients, which show a positive temperature dependence. However, the computed lower level (M06-2X/6-31+G**) rate coefficients agree better with these experimental values than the rate coefficients computed at the higher level (UCCSD(T*)F12ave/CBSave//M06-2X/6-31+G**). This type of discrepancy has been noted before (59). At present, with wavefunction methods, one can carry out systematic improvements in the computation of relative electronic barriers, with the geometries of the reactants, RC, TS, PC and products obtained at a lower level (M06-2X/6-31+G** in this case). In this connection, there is little more that we can do to improve the enthalpy of activation as UCCSD(T*)-F12-CBS is at present at the state-of-the-art level. (It should also be noted that it is inappropriate to compare computed activation energies with experimentally

derived activation energies; see our previous work (11,49,56)). Regarding geometrical structures and vibrational frequencies, a method with analytical first and second derivatives is required. We have previously shown that using different functionals for the lower level, for geometries and frequencies, with the same higher level barrier height can lead to computed rate coefficients which differ by one order of magnitude as the entropic contribution to the free energy of activation will be different with different functionals (11,49,56). In summary, one should bear in mind that the uncertainties associated with the entropic and/or enthalpic contributions can lead to computed uncertainties in the computed rate coefficients. Further theoretical and experimental investigations are required to bring theory closer to experiment for this reaction, with the evidence from the present work clearly favouring the lower set of experimental rate coefficients.

Acknowledgements

The authors are grateful to the Research Grant Council (RGC) of the Hong Kong Special Administrative Region (HKSAR, Grant Numbers: PolyU 5011/12P and 5018/13P), the Research Committee of the Hong Kong Polytechnic University (Account No. A-PK41 and G-YG99) and NERC (UK) for support, and the National Service for Computational Chemistry Software (NSCCS), EPSRC (UK) for computational resources.

References

1.Roberts J. M. The Atmospheric Chemistry of Organic Nitrates
Atmospheric Environment Part A-General Topics **1990**, *24*, 243-287.
2.Clemitshaw K. C., Williams J., Rattigan O. V., Shallcross D. E., Law K. S., and Cox, R. A. Gas-phase ultraviolet absorption cross-sections and atmospheric lifetimes of C2-C6 alkyl nitrates *J Photochem Photobiol A* **1997**, *102*, 117-126.
3.Ballschmiter K. Atmospheric chemistry: A marine source for alkyl nitrates
Science **2002**, *297*, 1127-1128.
4.Atlas E., Pollock W., Greenberg J., Heidt L., and Thompson A. M. Alkyl nitrates, non-methane hydrocarbons and halocarbon gases over the equatorial pacific-ocean during SAGA3 *Journal of Geophysical Research-Atmospheres* **1993**, *98*, 16933-16947.
5.Blake N. J., Blake D. R., Swanson A. L., Atlas E., Flocke F., and Rowland F. S. Latitudinal, vertical and seasonal variations of C1-C4 alkyl nitrates in the troposphere over the pacific ocean during PEM-Tropics A and B: Ocean and continental sources *Journal of Geophysical Research-Atmospheres* **2003**, *108*, 8242, Issue D2.
6.Chuck A. L., Turner S. M., and Liss P. S. Direct evidence for a marine source of C-1 and C-2 alkyl nitrates *Science* **2002**, *297*, 1151-1154.
7.Darnall K. R., Carter W. P. L., Winer A. M., Lloyd A. C., and Pitts J. N. Importance of RO_2 + NO in alkyl nitrate formation from C4-C6 alkane photooxidation under simulated atmospheric conditions *Journal of Physical Chemistry* **1976**, *80*, 1948-1950.
8. He S, Chen Z. and Zhang X. Photochemical reactions of methyl and ethyl nitrate: a dual role for alkyl nitrates in the nitrogen cycle *Environ. Chem*., 2011, **8**, 529-542
9. Wu S, Mickley J.L, Jacob D.J, Logan J.A, Yantosca R.M and Rind D. Why are there large differences between models in global budgets of tropospheric ozone? J.Geophys Res 112, 2007, D05302, Issue D5

10.Horowitz L.W, Fiore A.M, Milly G.P, Cohen R.C, Perring A, Wooldridge P.J, Hess P.G, Emmons L.K and Lamarque J.F. Observational constraints on the chemistry of isoprene nitrates over the eastern Unites States J.Geophys Res 112, 2007, D12S08, Issue D12

11. Ng M., Mok D.K.W., Lee E.P.F. and Dyke J.M. A theoretical study of the mechanism of the atmospherically relevant reaction of chlorine atoms with methyl nitrate, and calculation of the reaction rate coefficient at temperatures relevant to the troposphere PCCP 2015, 17, 7463-7476
12.Talukdar R.K., Burkholder J.B., Hunter M., Gilles M.K., Roberts J.M. and Ravishankara A.V. Atmospheric fate of several alkyl nitrates 1. Rate coefficients of the reactions of alkyl nitrates with isotopically labelled hydroxyl radicals J.C.S.Faraday 1997, 93, 2797-2805
13.Taylor W.D., Allston T.D., Moscato M.J., Fazekas G.B., Kozlowski R., and Takacs G.A. Atmospheric photo-dissociation lifetimes for nitromethane, methyl nitrite and methyl nitrate Int J. Chemical Kinetics 1980, 12, 231-240
14.Talukdar R. K., Herndon S. C., Burkholder J. B., Roberts, J. M. and Ravishankara A. R. Atmospheric fate of several alkyl nitrates 2. UV absorption cross-sections and photodissociation quantum yields *Journal of the Chemical Society-Faraday Transactions* **1997**, *93*, 2787-2796.
15.Shallcross D. E., Biggs P., CanosaMas C. E., Clemitshaw K. C., Harrison M. G., Alanon

M. R. L., Pyle J. A., Vipond, A.and Wayne R. P. Rate constants for the reaction between OH and CH_3ONO_2, and $C_2H_5ONO_2$ over a range of pressure and temperature *Journal of the Chemical Society-Faraday Transactions* **1997**, *93*, 2807-2811.
16.Gaffney J. S., Fajer R., Senum G. I., and Lee J. H. Measurement of the reactivity of OH with methyl nitrate--implications for prediction of alkyl nitrate –OH reaction rates *International Journal of Chemical Kinetics* **1986**, *18*, 399-407.
17. Kakesu, M.; Bandow H.,Takenaka N., Maeda Y., and Washida N. Kinetic measurements of methyl and ethyl nitrate reactions with OH radicals *International Journal of Chemical Kinetics* **1997**, *29*, 933-941.
18.Nielsen O. J., Sidebottom H. W., Donlon M.and Treacy J. An absolute-rate and relative-rate study of the gas-phase reaction of OH radicals and Cl atoms with normal alkyl nitrates *Chemical Physics Letters* **1991**, *178*, 163-170.
19.Kerr, J. A., and Stocker D. W. Kinetics of the reactions of hydroxyl radicals with alkyl nitrates and with some oxygen-containing organic-compunds studied under simulated atmospheric conditions *Journal of Atmospheric Chemistry* **1986**, *4*, 253-262.
20. Cox A.P. and Waring S. Microwave spectrum, structure and dipole moment of methyl nitrate Trans Far Soc 67, 1971, 3441-3449
21.Zhao Y. and Truhlar D. G. The M06 suite of density functionals for main group thermochemistry, thermochemical kinetics, noncovalent interactions, excited states, and transition elements: two new functionals and systematic testing of four M06-class functionals and 12 other functionals *Theoretical Chemistry Accounts* **2008**, *120*, 215-241.
22.Frisch M. J., Trucks G. W., Schlegel H. B., Scuseria G. E., Robb M. A., Cheeseman J. R., Scalmani G., Barone V., Mennucci B., Petersson G. A., Nakatsuji H., Caricato M., Li X., Hratchian H. P., Izmaylov A. F., Bloino J., Zheng, G., Sonnenberg J. L., Hada M., Ehara M., Toyot K., Fukuda R., Hasegawa J., Ishida M., Nakajima T., Honda Y., Kitao O., Nakai H., Vreven T., Montgomery J.J. A., Peralta J. E., Ogliaro F., Bearpark M., Heyd J. J., Brothers, E., Kudin K. N.,Staroverov V. N., Keith T., Kobayashi R., Normand J., Raghavachari K., Rendell A., Burant J. C., Iyengar S. S., Tomasi J., Cossi M., Rega N., Millam J. M., Klene M., Knox J. E., Cross J. B., Bakken V., Adamo C., Jaramillo J., Gomperts R., Stratmann R. E., Yazyev O., Austin A. J., Cammi R., Pomelli C., Ochterski J. W., Martin R. L., Morokuma K., Zakrzewski V. G., Voth G. A., Salvador P., Dannenberg J. J., Dapprich S., Daniels A. D., Farkas Ö., Foresman J. B., Ortiz J. V., Cioslowski J., and Fox D. J. Gaussian 09; Revision B.01 ed.; Gaussian, Inc.: Wallingford CT, 2010.
23.Goerigk L.and Grimme S. A thorough benchmark of density functional methods for general main group thermochemistry, kinetics and non-covalent interactions *Physical Chemistry Chemical Physics* **2011**, *13*, 6670-6688.
24.Zheng J. J., Zhao Y. and Truhlar, D. G. The DBH24/08 database and its use to assess electronic structure model chemistries for chemical reaction barrier heights *Journal of Chemical Theory and Computation* **2009**, *5*, 808--821.
25.Zhao Y., and Truhlar D. G. Density functionals with broad applicability in chemistry *Accounts of Chemical Research* **2008**, *41*, 157-167.
26.Xu X. F., Alecu I. M. and Truhlar D. G. How well can modern density functionals predict internuclear distances at transition states? *Journal of Chemical Theory and Computation* **2011**, *7*, 1667-1676.
27.Hratchian H. P. and Schlegel, H. B. Accurate reaction paths using a Hessian predictor-corrector integrator *Journal of Chemical Physics* **2004**, *120*, 9918-9924.
28.Hratchian H. P., and Schlegel H. B. Finding minima, transition states, and following reaction pathways on ab initio potential energy surfaces. In *Theory and Applications of Computational Chemistry: The First Forty Years*; Dykstra, C. E., Frenking, G., Kim, K. S., Scuseria, G. E., Eds.; Elsevier: Amsterdam, 2005; pp 195-249.

29.Hratchian H. P., and Schlegel H. B. Using Hessian up-dating to increase the efficiency of a Hessian based predictor-corrector reaction path following method *Journal of Chemical Theory and Computation* **2005**, *1*, 61-69.
30.Knizia, G., Adler, T. B., and Werner, H. J. Simplified CCSD(T)-F12 methods: theory and benchmarks *Journal of Chemical Physics* **2009**, *130*, 054104.
31.Werner H. J., Knizia G.and Manby F. R. Explicitly correlated coupled cluster methods with pair-specific geminals *Mol Phys* **2011**, *109*, 407-417.
32.Werner H.-J., Knowles P. J., Knizia G., Manby F. R., Schütz M., Celani P., Korona T., Lindh R., Mitrushenkov A., Rauhut G., Shamasundar K. R., Adler T. B., Amos R. D., Bernhardsson A., Berning A., Cooper D. L., Deegan M. J. O., Dobbyn A. J., Eckert F., Goll E., Hampel C., Hesselmann A., Hetzer G., Hrenar T., Jansen G., Köppl C., Liu Y., Lloyd A. W., Mata R. A., May A. J., McNicholas S. J., Meyer W., Mura M. E., Nicklass A., O'Neill D. P., Palmieri P., Peng D., Pflüger K., Pitzer R., Reiher M., Shiozaki T., Stoll H., Stone A. J., Tarroni R., Thorsteinsson T., and Wang M. MOLPRO, version 2012.1, a package of ab initio programs.
33.Werner H. J., Knowles P. J., Knizia G., Manby F. R.and Schutz M. MOLPRO:a general purpose quantum chemistry program package *Wiley Interdisciplinary Reviews- Comput Mol Sci* **2012**, *2*, 242-253.
34.Peterson K. A., Adler T. B., and Werner, H. J. Systematically convergent basis sets for explicitly correlated wavefunctions: The atoms H,He,B-Ne and Al-Ar *Journal of Chemical Physics* **2008**, *128*, 084102.
35.Weigend F., Kohn A., and Hattig C. Efficient use of the correlation consistent basis sets in resolution of the identity MP2 calculations *Journal of Chemical Physics* **2002**, *116*, 3175-3183.
36.Helgaker T., Klopper W., Koch H., and Noga J. Basis-set convergence of correlated calculations on water *Journal of Chemical Physics* **1997**, *106*, 9639-9646.
37.Halkier A., Helgaker T., Klopper W., Jorgensen P; and Csaszar A. G. Comment on "Geometry optimization with an infinite basis set" (J.Phys Chem A103, 1999, 651) and "Basis set exptrapolation " (Chem Phys Letts 294, 1988, 45) *Chemical Physics Letters* **1999**, *310*, 385-389.
38.Schwenke D. W. The extrapolation of one-electron basis sets in electronic structure calculations. How it should work and how it can be made to work. *Journal of Chemical Physics* **2005**, *122*, 014107.
39.Hill J. G., Peterson K. A., Knizia G.and Werner, H. J. Extrapolating MP2 and CCSD explicitly correlated energies to the complete basis set limit with first and second row correlation consistent basis sets *Journal of Chemical Physics* **2009**, *131*, 194105.
40.Li G. X., Gao T., Chen D., Li Y. X.; Zhang Y. G. and Zhu Z. H.The splitting of low-lying states for the hydroxyl molecule under spin-orbit splitting *Chinese Phys* **2006**, *15*, 998-1003.
41.Zheng J., Zhang S., Lynch B. J., Corchado J. C., Chuang Y.-Y., Fast P. L., Hu W.-P., Liu Y.-P., Lynch G. C., Nguyen K. A., Jackels C. F., Fernández Ramos A., Ellingson B. A., Melissas V. S., Villà J., Rossi I., Coitiño E. L.,Pu J., Albu T. V., Steckler R., Garrett B. C., Isaacson A. D. and Truhlar D. G. POLYRATE 2010-A; 2010 ed.; Department of Chemistry and Supercomputing Institute, University of Minnesota: Minneapolis, Minnesota, 2010.
42.Truhlar D. G. A simple approximation for the vibrational partition-function of a hindered internal-rotation *Journal of Computational Chemistry* **1991**, *12*, 266-270.
43.Chuang Y. Y.; and Truhlar D. G. Statistical thermodynamics of bond torsional modes *Journal of Chemical Physics* **2000**, *112*, 1221-1228.
44.Ellingson B. A., Lynch V. A., Mielke S. L. and Truhlar D. G. Statistical thermodynamics of bond torsional modes: Tests of separable, almost separable and improved Pitzer-Gwinn approximations *Journal of Chemical Physics* **2006**, *125, 084305*.

45.Garrett B. C., Redmon M. J., Steckler R., Truhlar D. G., Baldridge K. K., Bartol D., Schmidt M. W., and Gordon M. S. Algorithms and accuracy requirements for computing reaction paths by the method of steepest descent *Journal of Physical Chemistry* **1988**, *92*, 1476-1488.
46.Nguyen K. A., Jackels C. F., and Truhlar, D. G. Reaction-path dynamics in curvilinear internal coordinates including torsions *Journal of Chemical Physics* **1996**, *104*, 6491-6496.
47.Chuang Y. Y.and Truhlar D. G. Reaction path dynamics in redundant internal coordinates *Journal of Physical Chemistry A* **1998**, *102*, 242-247.
48.Chuang Y. Y., Corchado J. C., and Truhlar, D. G. Mapped interpolation scheme for single-point energy corrections in reaction path calculations and a critical evaluation of dual –level reaction path dynamics methods *Journal of Physical Chemistry A* **1999**, *103*, 1140-1149.
49.Chow R., Ng, M., Mok D. K. W., Lee E. P. F.and Dyke J. M. Rate coefficients of the Cl + $CH_3C(O)OCH_3$ $\rightarrow$ HCl + $CH_3C(O)OCH_2$ reaction at different temperatures calculated by transition-state theory with ab initio and density functional theory reaction paths *Journal of Physical Chemistry A* **2014**, *118*, 2040-2055.
50. Burcat A., and Ruscic B. Third Millennium Ideal Gas and Condensed Phase Thermochemical Database for Combustion with updates from Active Thermochemical Tables; Aerospace Engineering, and Argonne National Laboratory, Chemistry Division, 2005; Vol. ANL-05/20 and TAE 960 Technion-IIT.
51. Ruscic B., Pinzon R. E., Morton M. L., Srinivasan N. K., Su M. C., Sutherland J. W. and Michael J. V. Active thermochemical tables:accurate enthalpy of formation of the hydroperoxy radical HO_2 *Journal of Physical Chemistry A* **2006**, *110*, 6592-6601.
52. Cox J. D., Wagman D. D. and Medvedev V. A. *CODATA Key Values for Thermodynamics*; Hemisphere: New York, 1984.
53. Garrett B. C., Truhlar D. G., Grev R. S. and Magnuson A. W. Improved treatment of threshold contributions in variational transition-state theory *Journal of Physical Chemistry* **1980**, *84*, 1730-1748.
54. Fernandez-Ramos A., Ellingson B. A., Garrett B. C., and Truhlar D. G. Variational transition state theory with multidimensional tunneling. In *Reviews in Computational Chemistry*; Lipkowitz K. B., Cundari T. R., Eds.; Wiley-VCH: Hoboken, NJ, 2007; Vol. 23; pp 125.
55. Garrett B. C. and Truhlar D. G. Generalised transition state theory calculations for the reactions D + H_2 and H + D_2 using an accurate potential energy surface: explanation of the kinetic isotope effect *Journal of Chemical Physics* **1980**, *72*, 3460-3471.
56..M. Ng, D. K. W. Mok, E.P. F. Lee, and J. M. Dyke A theoretical investigation of the atmospherically important reaction between chlorine atoms and formic acid: determination of the reaction mechanism and calculation of the rate coefficient at different temperatures Molecular Physics 113, 2015, 1511-1533
57. C. J. Young, R. A. Washenfelder, P. M. Edwards, D. D. Parrish, J. B. Gilman, W. C. Kuster, L. H. Mielke, H. D. Osthoff, C. Tsai, O. Pikelnaya, J. Stutz, P. R. Veres, J. M. Roberts, S. Griffith, S. Dusanter, P. S. Stevens, J. Flynn, N. Grossberg, B. Lefer, J. S. Holloway, J. Peischl, T. B. Ryerson, E. L. Atlas, D. R. Blake and S. S. Brown Chlorine as a primary radical: evaluation of methods to understand its role in initiation of oxidative cycles *Atmos. Chem. Phys*., 2014, **14**, 3427-3440.
58.B.J. Finlayson-Pitts and J.N. Pitts Jr., *Chemistry of the Upper and Lower Atmosphere* (Academic Press, San Diego, 2000)
59. J.Zheng and D.G.Truhlar Multi-path variational transition state theory for chemical reaction rates of complex polyatomic species: ethanol + OH Faraday Discussions 157, 2012, 59-88
60. Khursan S. L. and Martem'yanov V. S. Thermochemistry of peroxy radical

recombination *Russian Journal of Physical Chemistry* **1991**, *65*, 321-330.
61.Sander S. P., Abbatt J., Barker, J. R., Burkholder, J. B.,Friedl, R. R.,Golden, D. M., Huie R. E., Kolb C. E., Kurylo M. J., Moortgat G. K., Orkin V. L.and Wine, P. H. Chemical Kinetics and Photochemical Data for Use in Atmospheric Studies; JPL Publication 10-6, Jet Propulsion Laboratory: Pasadena, 2011; Vol. Evaluation No. 17.
62. Hine J.and Arata K. *B* Keto-enol tautomerism 2. Calorimetrical determination of equilibrium constansts for keto-enol tautomerism of cyclohexane and acetone *Chem Soc Jpn* **1976**, *49*, 3089-3092.
63. Baroody E. E.and Carpenter G. A. Heats of formation of propellant compounds; Rpt. Naval Ordnance Systems Command Task No. 331-003/067-1/UR2402-001 for Naval Ordance Station, Indian Head, MD, 1972; pp 1.
64.Chao J. and Rossini F. D. Heats of combustion, formation and isomerization of nineteen alkanols *Journal of Chemical and Engineering Data* **1965**, *10*, 374-379.
65.Green J. H. S. Revision of the values of the heats of formation of normal alcohols *Chemistry and Industry* **1960**, 1215-1216.
66. Parks G. S. Thermal data on organic compounds I. The heat capacities and free energies of methyl, ethyl and normal-butyl alcohols *Journal of the American Chemical Society* **1925**, *47*, 338-345.
67.Richards T. W. and Davis H. S. The heats of combustion of benzene, toluene, aliphatic alcohols, cyclhexanol and other carbon compounds *Journal of the American Chemical Society* **1920**, *42*, 1599-1617.
68.Chase M. W. Jr.
Journal of Physical and Chemical Reference Data **1998**, 27, issue 6, 1-2.
69.Huber K. P. and Herzberg G. "Constants of diatomic molecules" in NIST Chemistry WebBook, NIST Standard Reference Database 69, National Institute of Standards and Technology.
70.Tsang W. Heats of formation of organic free radicals by kinetic methods. In *Energetics of Organic Free Radical*; Martinho Simoes, J. A., Greenberg, A., Liebman, J. F., Eds.; Blackie Academic and Professional: London, 1996, 22-58.
71. I.Wadso Heats of vaporization for a number of organic compounds
Acta Chemica Scandinavica 1966, 20, 544-532

.

Table 1. Computed reaction (ΔE_e^{RX}) and activation ($\Delta E_e^{\ddagger}$) energies (in kcal mol^{-1}) of the OH + CH_3ONO_2 → TS_2 → CH_3OOH + NO_2 channel at various UCCSD(T*)-F12x//M06-2X/6-31+G** levels of calculation.

Methods	ΔE_e^{RX}			$\Delta E_e^{\ddagger}$		
	F12a	F12b	(other)	F12a	F12b	(other)
(M06-2X/6-31+G**)			(0.28)			(29.86)
UCCSD(T*)-F12x/VTZ-F12	-1.810	-1.746		23.384	23.562	
UCCSD(T*)-F12x/VQZ-F12	-1.757	-1.725		23.822	23.904	
$1/X^3$ CBS1	-1.718	-1.710		24.141	24.153	
Schwenke CBS2	-1.737	-1.718		23.981	24.028	
Average ΔE_e (CBS1 and CBS2)	-1.728	-1.714		24.061	24.090	
Best ΔE_e (F12ave/CBSave)[a]			-1.72(1)			24.08(17)
ΔE_{0K} (CBSave)	-1.416	-1.402		24.348	24.378	
ΔE_{0K} (include SO of OH)	-1.216	-1.202		24.548	24.578	
Best ΔE_{0K} (F12ave/CBSave)[a]			-1.21			24.56
ΔH_{298K}	-1.365	-1.352				
ΔH_{298K} (including SO of OH)	-1.165	-1.152				
Best ΔH_{298K} (F12ave/CBSave)[a]			-1.16			
ΔH_{298K} (from available $\Delta H_{f,298K}$)			-2.96[b] -2.41[c]			

[a] The average of four CBS values (uncertainties w.r.t. F12b/VQZ-F12 values).

[b] Using $\Delta H_{f,298K}$ values of CH_3ONO_2, -29.16 kcal mol^{-1};[50] OH, 8.93 kcal mol^{-1};[51] CH_3OOH, -31.31 kcal mol^{-1};[60] NO_2, 8.12 kcal mol^{-1}.[51,61]

[c] Using the $\Delta H_{f,298K}$ value of -29.71 kcal mol^{-1}, which was computed in our previous study,[11] for CH_3ONO_2 instead of the value from Burcat[50] given in footnote (b).

Table 2. Computed reaction (ΔE_e^{RX}) and activation ($\Delta E_e^{\ddagger}$) energies (in kcal mol^{-1}) of the OH + CH_3ONO_2 → TS_3 → CH_3OH + NO_3 channel at various UCCSD(T*)-F12x//M06-2X/6-31+G** levels of calculation.

Methods	ΔE_e^{RX}			$\Delta E_e^{\ddagger}$		
	F12a	F12b	(other)	F12a	F12b	(other)
(M06-2X/6-31+G**)			(-2.21)			(37.71)
UCCSD(T*)-F12x/VTZ-F12	-8.311	-8.328		35.643	35.755	
UCCSD(T*)-F12x/VQZ-F12	-8.106	-8.109		35.915	35.966	
$1/X^3$ CBS1	-7.956	-7.949		36.114	36.120	
Schwenke CBS2	-8.031	-8.029		36.014	36.043	
Average ΔE_e (CBS1 and CBS2)	-7.994	-7.989		36.064	36.081	
Best ΔE_e (F12ave/CBSave)[a]			-7.99(12)			36.07(11)
ΔE_{0K} (CBSave)	-7.931	-7.926		36.884	36.902	
ΔE_{0K} (include SO of OH)	-7.731	-7.726		37.084	37.102	
Best ΔE_{0K} (F12ave/CBSave)[a]			-7.73			37.09
ΔH_{298K}	-8.212	-8.207				
ΔH_{298K} (including SO of OH)	-8.012	-8.007				
Best ΔH_{298K} (F12ave/CBSave)[a]			-8.01			
ΔH_{298K} (from available $\Delta H_{f,298K}$)			-11.77[b] -11.22[c] -9.83[c,d]			

[a] The average of four CBS values (uncertainties w.r.t. F12b/VQZ-F12 values).

[b] Using $\Delta H_{f,298K}$ values of CH_3ONO_2, -29.16 kcal mol^{-1};[50] OH, 8.93 kcal mol^{-1};[51] CH_3OH, -49.0 kcal mol^{-1}(average of nine values);[62-67] NO_3, 17.0 kcal mol^{-1}.[68]

[c] Using the $\Delta H_{f,298K}$ value of -29.71 kcal mol^{-1}, which was computed in our previous study,[11] for CH_3ONO_2 instead of the value from Burcat[50] given in footnote (b).

[d] Using the $\Delta H_{f,298K}$ value of -47.61 kcal mol^{-1}, which was computed in the present study, for CH_3OH instead of the average of nine values given in footnote (b).

Table 3. Computed reaction energies (ΔE_e^{RX}; in kcal mol^{-1}) obtained at different levels of calculation for the $CH_3OH \rightarrow CO + 2H_2$ reaction, and the derived $\Delta H_{f,298K}$ value for CH_3OH.

ΔE_e^{RX}	UCCSD(T*)-F12a	UCCSD(T*)-F12b
VTZ-F12	34.11	34.03
VQZ-F12	34.40	34.36
1/X^3 CBS1	34.61	34.60
Schwenke CBS2	34.50	34.48
Best estimate (F12ave/CBSave)[a]		34.55
ΔE_{0K}^{RX} (ΔZPE = -16.90 kcal mol^{-1})		17.65
ΔH_{298K}^{RX} [b]		21.20
$\Delta H_{f,298K}(CH_3OH)$[c]		-47.61
Experimental $\Delta H_{f,298K}(CH_3OH)$		-48.0,[d] -47.94,[e] -48.1 ± 1.2,[f] -48.21,[g] -48.33 ± 0.05,[h] -48.07 ± 0.05,[i] -50.86,[j] -50.98 ± 0.48,[k] -51.1 ± 1.2[l]

[a] The average of the four UCCSD(T*)-F12x/CBS values.

[b] ΔZPE + ΔE_v^{298K} + 6.5RT = -13.35 kcal mol^{-1}.

[c] Using $\Delta H_{f,298K}(CO)$ = -26.417 ± 0.041 kcal mol^{-1} and the computed best F12ave/CBSave ΔH_{298K}^{RX} of 21.20 kcal mol^{-1}.

[d] From Ref. [62].

[e] Value computed using $\Delta H_{f,liquid}°$ of -238.4 kJ mol^{-1} from Ref. [63] and $\Delta H_{vap}°$ of 37.8 kJ mol^{-1} from Ref. [65].

[f] Value computed using $\Delta H_{f,liquid}°$ of -238.4 kJ mol^{-1} from Ref. [63] and $\Delta H_{vap}°$ of 8.91 kcal mol^{-1} from Ref. [71].

[g] Value computed using $\Delta H_{f,liquid}°$ of -239.5 ± 0.2 kJ mol^{-1} from Ref. [64] and $\Delta H_{vap}°$ of 37.8 kJ mol^{-1} from Ref. [65].

[h] Value computed using $\Delta H_{f,liquid}°$ of -238.4 kJ mol^{-1} from Ref. [64] and $\Delta H_{vap}°$ of 8.91 kcal mol^{-1} from Ref. [71].

[i] From Ref. [65].

[j] Value computed using $\Delta H_{f,liquid}°$ of -250.6 kJ mol^{-1} from Ref. [66] and $\Delta H_{vap}°$ of 37.8 kJ mol^{-1} from Ref. [65].

[k] Value computed using $\Delta H_{f,liquid}°$ of -250.6 kJ mol^{-1} from Ref. [66] and $\Delta H_{vap}°$ of 8.91 kcal mol^{-1} from Ref. [71].

[l] Value computed using $\Delta H_{f,liquid}°$ from Ref. [67] and $\Delta H_{vap}°$ of 8.91 kcal mol^{-1} from Ref. [71].

Table 4. Computed reaction (ΔE_e^{RX}) and activation ($\Delta E_e^{\ddagger}$) energies (in kcal mol^{-1}) of the OH + CH_3ONO_2 → TS_{4a} → CH_3O + HNO_3 channel at various UCCSD(T*)-F12x//M06-2X/6-31+G** levels of calculation.

Methods	ΔE_e^{RX}			$\Delta E_e^{\ddagger}$		
	F12a	F12b	(other)	F12a	F12b	(other)
(M06-2X/6-31+G**)			(-7.32)			(31.88)
UCCSD(T*)-F12x/VTZ-F12	-6.472	-6.512		26.485	26.635	
UCCSD(T*)-F12x/VQZ-F12	-6.544	-6.558		27.007	27.060	
$1/X^3$ CBS1	-6.597	-6.591		27.388	27.369	
Schwenke CBS2	-6.570	-6.574		27.197	27.214	
Average ΔE_e (CBS1 and CBS2)	-6.583	-6.583		27.293	27.291	
Best ΔE_e (F12ave/CBSave)[a]			-6.58(3)			27.29(17)
ΔE_{0K} (CBSave)	-6.528	-6.527		28.622	28.620	
ΔE_{0K} (include SO of OH)	-6.328	-6.327		28.822	28.820	
Best ΔE_{0K} (F12ave/CBSave)[a]			-6.33			28.82
ΔH_{298K}	-6.980	-6.979				
ΔH_{298K} (including SO of OH)	-6.780	-6.779				
Best ΔH_{298K} (F12ave/CBSave)[a]			-6.78			
ΔH_{298K} (from available $\Delta H_{f,298K}$)			-7.77[b] -7.22[c]			

[a] The average of four CBS values (uncertainties w.r.t. F12b/VQZ-F12 values).

[b] Using $\Delta H_{f,298K}$ values of CH_3ONO_2, -29.16 kcal mol^{-1};[50] OH, 8.93 kcal mol^{-1};[51] CH_3O, 4.1 kcal mol^{-1};[70] HNO_3, -32.101 kcal mol^{-1}.[68]

[c] Using the $\Delta H_{f,298K}$ value of -29.71 kcal mol^{-1}, which was computed in our previous study,[11] for CH_3ONO_2 instead of the value from Burcat[50] given in footnote (b).

Table 5. Computed ΔE_e, ΔE_{0K} and ΔH_{298K} (w.r.t. separate reactants; in kcal mol^{-1}) of various species in the OH + CH_3ONO_2 → TS_{4b} → $CH_3O(OH)NO_2$ conformer 1 → TS_{rot} → $CH_3O(OH)NO_2$ conformer 2 → TS_{4c} → CH_3O + HNO_3 channel obtained at various UCCSD(T*)-F12x//M06-2X/6-31+G** levels of calculation.

ΔE_e (in kcal mol^{-1})	**TS_{4b}**	**$CH_3O(OH)NO_2$ conformer 1**	**TS_{rot}**	**$CH_3O(OH)NO_2$ conformer 2**	**TS_{4c}**	**Δ(RX)**
M06-2X/6-31+G**	30.86	21.67	23.53	20.16	28.48	-7.32
UCCSD(T*)-F12a/VTZ-F12	31.95	25.56	27.22	23.74	30.44	-6.47
UCCSD(T*)-F12b/VTZ-F12	32.06	25.68	27.35	23.86	30.54	-6.51
UCCSD(T*)-F12a/VQZ-F12	32.15	25.58	27.24	23.74	30.58	-6.54
UCCSD(T*)-F12b/VQZ-F12	32.18	25.62	27.29	23.78	30.61	-6.56
UCCSD(T*)-F12a/CBS1	32.30	25.59	27.26	23.75	30.69	-6.60
UCCSD(T*)-F12b/CBS1	32.27	25.57	27.24	23.73	30.66	-6.59
UCCSD(T*)-F12a/CBS2	32.22	25.58	27.25	23.74	30.64	-6.57
UCCSD(T*)-F12b/CBS2	32.23	25.60	27.26	23.76	30.64	-6.57
Best ΔE_e (F12ave/CBSave)[a]	32.25(7)	25.59(3)	27.25(3)	23.74(4)	30.66(5)	-6.58(3)
Δ(ZPE)	1.97	3.09	3.04	3.21	1.77	0.06
ΔE_{0K} (= best ΔE_e + ΔZPE)	34.22	28.68	30.30	26.95	32.42	-6.53
ΔE_{0K} (include SO of OH)	34.42	28.88	30.50	27.15	32.62	-6.33
ΔH_{298K}		27.44		25.76		-6.98
ΔH_{298K} (include SO of OH)		27.64		25.96		-6.78
ΔH_{298K} (using $\Delta H_{f,298K}$ values)[b]						-7.77

[a] The average of four CBS values (uncertainties w.r.t. F12b/VQZ-F12 values).

[b] Using $\Delta H_{f,298K}$ values of CH_3ONO_2, -29.16 kcal mol^{-1};[50] OH, 8.93 kcal mol^{-1};[51] CH_3O, 4.1 kcal mol^{-1};[70] HNO_3, -32.101 kcal mol^{-1}.[68]

Table 6. Some major geometrical parameters (bond distance; in Å), the imaginary vibrational frequencies (ω_i; in cm^{-1}), the ΔE_e, ΔE_{0K} (w.r.t. separate reactants; in kcal mol^{-1}) and the zero-point energy correction {Δ(ZPE); in kcal mol^{-1}} of the three TS's in the OH + CH_3ONO_2 → H_2O + CH_2ONO_2 channel.

ΔE_e (in kcal mol^{-1})	TS_{1a}	TS_{1b}	TS_{1c}
ω_i[a]	1294i	1135i	1486i
C···H bond distance	1.20	1.19	1.22
H···O bond distance	1.33	1.36	1.29
L = Δ(C-H)/Δ(H-O)	0.39	0.25	0.39
M06-2X/6-31+G**	3.01	5.10	6.23
UCCSD(T*)-F12a/VTZ-F12	3.88	5.39	6.94
UCCSD(T*)-F12b/VTZ-F12	3.88	5.39	6.93
UCCSD(T*)-F12a/VQZ-F12	3.98	5.48	7.01
UCCSD(T*)-F12b/VQZ-F12	3.97	5.47	7.00
UCCSD(T*)-F12a/CBS1	4.04	5.55	7.06
UCCSD(T*)-F12b/CBS1	4.03	5.53	7.05
UCCSD(T*)-F12a/CBS2	4.01	5.51	7.04
UCCSD(T*)-F12b/CBS2	4.00	5.50	7.03
Best ΔE_e (F12ave/CBSave)[b]	4.02	5.52	7.05
Δ(ZPE)[c]	-1.46	-1.70	-2.20
ΔE_{0K} (= best ΔE_e + ΔZPE)	2.56	3.82	4.84
ΔE_{0K} (include SO of OH)[d]	2.76	4.02	5.04

[a] Computed at the M06-2X/6-31+G** geometries.

[b] The average of four CBS values (uncertainties w.r.t. F12b/VQZ-F12 values).

[c] Using computed M06-2X/6-31+G** harmonic frequencies.

[d] Including spin-orbit splitting in OH (0.40 kcal mol^{-1} = 0.0006 Hartree), the $^2\Pi_{3/2}$ SO state of OH is lower than the unperturbed $^2\Pi$ state by 0.20 kcal mol^{-1}.

Table 7. Computed ΔE_e, ΔE_{0K} and ΔH_{298K} (w.r.t. separate reactants; in kcal mol^{-1}) of various species in the out-of-plane OH + CH_3ONO_2 → H_2O + CH_2ONO_2 channel 1(a) obtained at various UCCSD(T*)-F12x//M06-2X/6-31+G** levels of calculations.

ΔE_e (in kcal mol^{-1})	**RC_{1a}**	**TS_{1a}**	**PC_{1a}**	**Δ(RX)**
M06-2X/6-31+G**	-5.41	3.01	-20.34	-14.63
UCCSD(T*)-F12a/**VTZ-F12**	-3.05	3.88	-20.34	-17.02
UCCSD(T*)-F12b	-3.03	3.88	-20.34	-17.02
UCCSD(T*)-F12a/**VQZ-F12**	-3.02	3.98	-20.46	-17.16
UCCSD(T*)-F12b	-3.02	3.97	-20.45	-17.15
UCCSD(T*)-F12a/CBS1[a]	-3.00	4.04	-20.54	-17.27
UCCSD(T*)-F12b/CBS1[a]	-3.01	4.03	-20.53	-17.24
UCCSD(T*)-F12a/CBS2[b]	-3.01	4.01	-20.50	-17.21
UCCSD(T*)-F12b/CBS2[b]	-3.02	4.00	-20.49	-17.20
Best ΔE_e (F12ave/CBSave)[c]	-3.01(1)	4.02(5)	-20.51(7)	-17.23(8)
Δ(ZPE)[d]	1.11	-1.46	-0.03	-1.31
ΔE_{0K} (= best ΔE_e + ΔZPE)	-1.91	2.56	-20.54	-18.54
ΔE_{0K} (include SO of OH)[e]	-1.71	2.76	-20.34	-18.34
Experimentally derived $\Delta E^{\ddagger}$		1.20[f] 2.03[g]		
ΔH_{298K}	-1.94	1.62	-20.00	-18.10
ΔH_{298K} (include SO of OH)[e]	-1.74	1.82	-19.80	-17.90
ΔH_{298K} (using $\Delta H_{f,298K}$ values)				-13.92,[h] -17.72[i]

[a] Using the $1/X^3$ CBS extrapolation of the ΔE_e at the UCCSD(T*)-F12/VTZ-F12 and UCCSD(T*)-F12/VQZ-F12 levels.

[b] Using the generalized two point CBS expression of Schwencke (38) {$E_{CBS}=(E_{large}-E_{small})F+E_{small}$, with F = 1.363388 from Hill et al.(39)} with the UCCSD(T*)-F12/VTZ-F12 and VQZ-F12 values.

[c] The best CBS estimate is the average of all the four CBS values and the estimated uncertainties are the differences between the best estimates and the UCCSD(T*)-F12b/VQZ-F12 values.

[d] Using computed M06-2X/6-31+G** harmonic frequencies.

[e] Including spin-orbit splitting in OH (0.40 kcal mol^{-1} = 0.0006 Hartree), the $^2\Pi_{3/2}$ SO state of

OH is lower than the unperturbed $^2\Pi$ state by 0.20 kcal mol^{-1}.

[f] Determined experimentally in Ref. [15].

[g] Determined experimentally in Ref. [14].

[h] Using $\Delta H_{f,298K}$ values of CH_3ONO_2, -29.16 kcal mol^{-1};[50] OH, 8.93 kcal mol^{-1};[51] CH_2ONO_2, 23.65 kcal mol^{-1};[50] H_2O, -57.7978 kcal mol^{-1}.[52]

[i] Using the $\Delta H_{f,298K}$ values of -29.71 and 19.30 kcal mol^{-1} for CH_3ONO_2 and CH_2ONO_2 respectively, which were computed in our previous study,[11] instead of the values from Burcat[50] given in footnote (f).

Table 8.

Comparison of computed $k^{ICVT/SCT}$ values {cm^3 $molecule^{-1}$ s^{-1}; $k^{ICVT/SCT} = 2k(1a) + 2k(1b) + k(1c)$} of the OH + CH_3ONO_2 → H_2O + CH_2ONO_2 reaction (column 2 and 3) at different temperatures obtained with the HL UCCSD(T*)-F12ave/CBSave//M06-2X IRC and available experimental values. Column 3 obtained with $\Delta E_e^{\ddagger}$ values 4.22 (1a), 5.72 (1b) and 7.25 (1c) kcal.mol^{-1} and column 2 obtained with these values reduced by 2.5 kcal.mol^{-1} (see text).

T (K)	$k_{ICVT/SCT}$	$k_{ICVT/SCT}$	Nielsen[a]	Kerr[b]	Gaffney[c]	Talukdar[d]	Kakesu[e]	Shallcross[f]
200	9.98E-15	9.07E-17						
220	1.38E-14	1.70E-16						
221						8.12E-15		
225						8.81E-15		
240	1.88E-14	3.04E-16						
250						1.39E-14		
260	2.52E-14	5.20E-16						
275						2.01E-14		
280	3.32E-14	8.55E-16						
290								
298	4.19E-14	1.29E-15	2.99E-13		3.40E-14			5.40E-14
300	4.29E-14	1.35E-15	2.93E-13			2.74E-14		5.48E-14
303				3.70E-13				
304							3.00E-14	
320	5.47E-14	2.06E-15						
325			2.23E-13			3.56E-14		6.39E-14
340	6.87E-14	3.06E-15						
350			1.77E-13			4.45E-14		7.30E-14
358								
360	8.52E-14	4.40E-15						
375			1.45E-13			5.40E-14		8.19E-14
380	1.04E-13	6.17E-15						
393			1.28E-13					
400	1.26E-13	8.47E-15				6.41E-14		9.06E-14
414						6.98E-14		
423								9.84E-14

[a] From Ref. [18]; rate coeffs. calculated from Arrhenius expression provided

[b] From Ref. [19].

[c] From Ref. [16].

[d] From Ref. [14]; rate coeffs. calculated from Arrhenius expression provided

[e] From Ref. [17];

[f] From Ref. [15]; rate coeffs. calculated from Arrhenius expression provided

Figure 1. Optimized geometries of the TS's at the M06-2X/6-31+G** level.

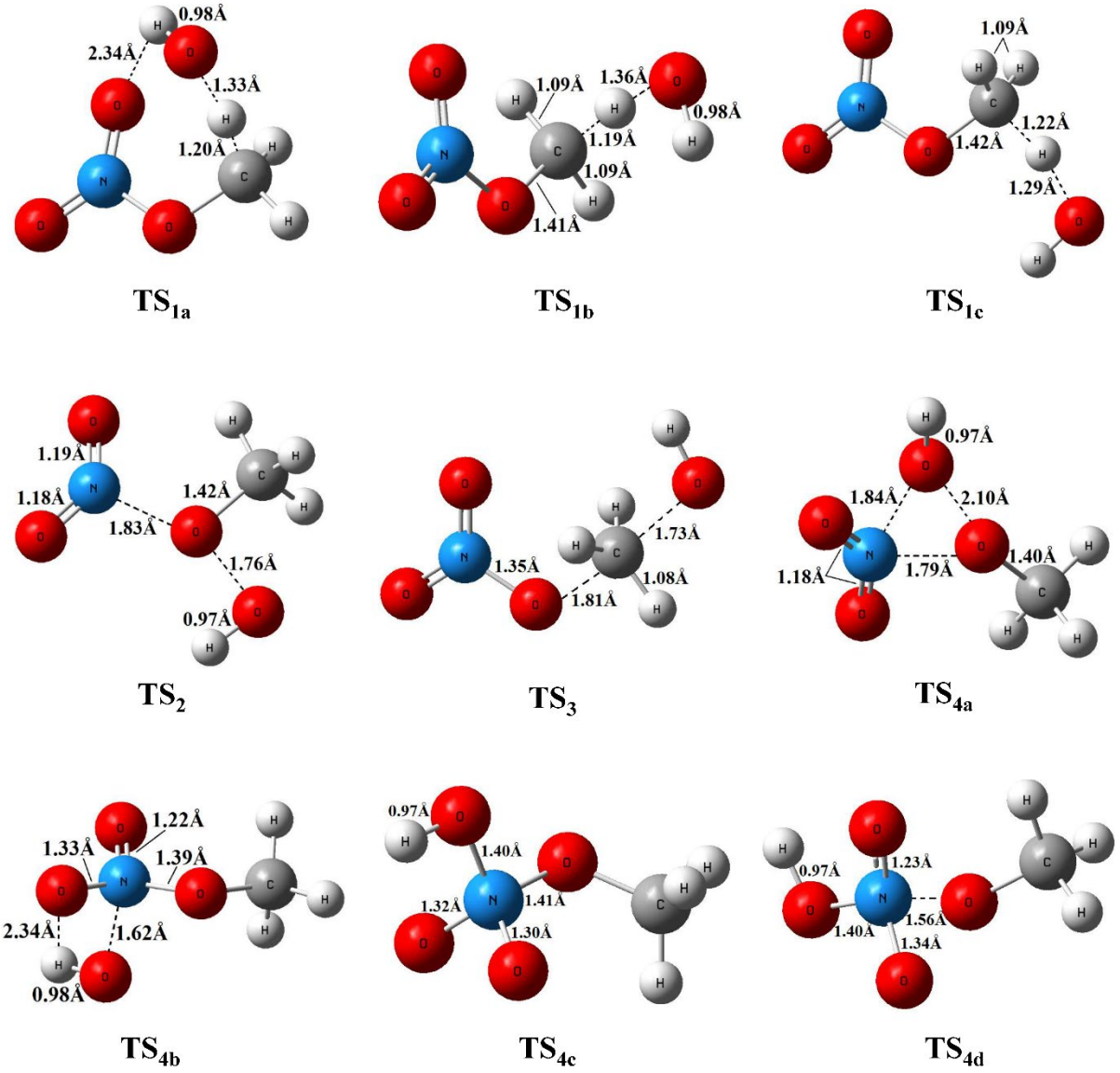

Figure 2. Optimized geometries of the adduct conformers in channel (4) and the complexes associated with TS_{1a} in channel (1) at the M06-2X/6-31+G** level. The reaction complexes through TS_{1a}, TS_{1b} and TS_{1c} have been optimised for reaction 1 and were considered in the rate coefficient calculations. Reactions 1a and 1b share the same reaction complex. For clarity only the reaction complex (RC_{1a}) is shown in this figure.

TheT

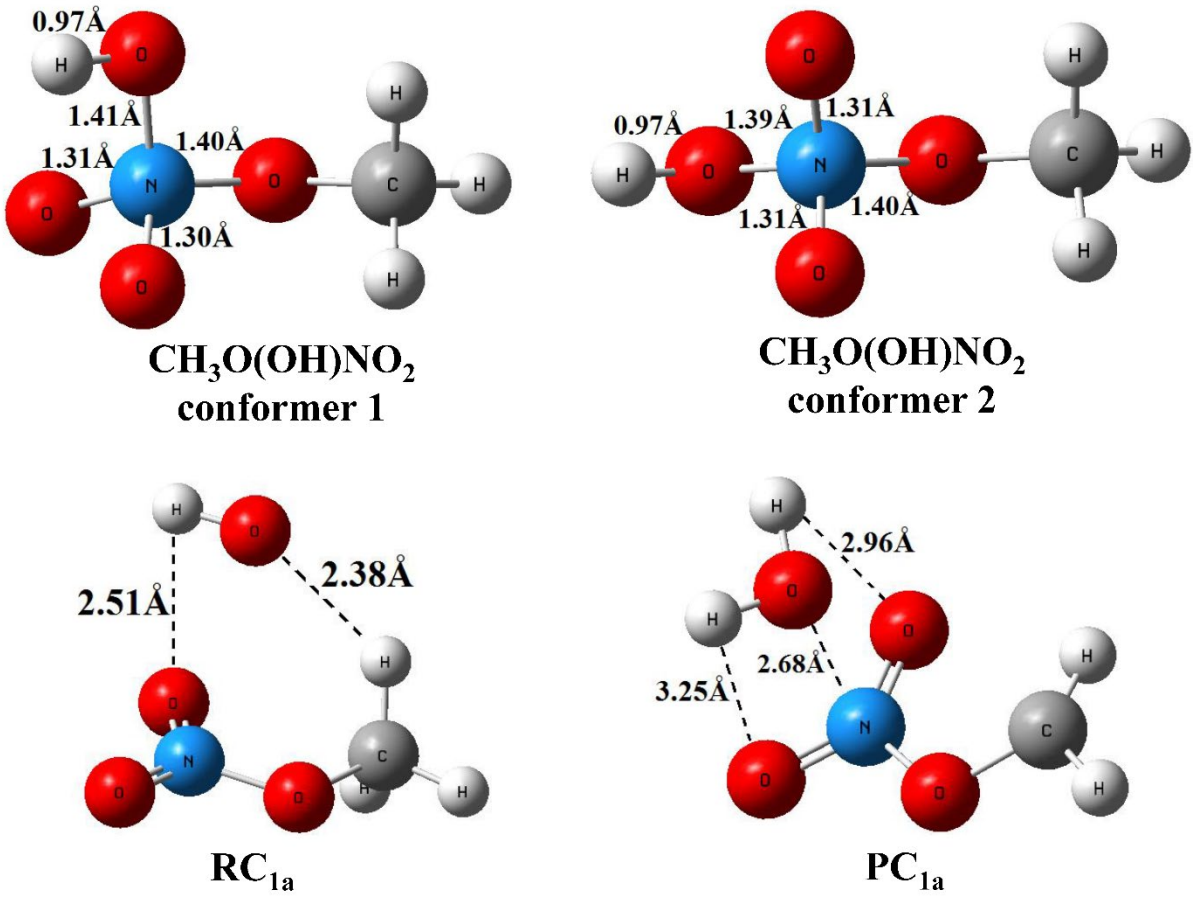

Figure 3. A schematic potential energy surface of the OH + CH_3ONO_2 reaction at the UCCSD(T*)-F12ave/CBSave//M06-2X level, including the ZPE and the SO corrections.

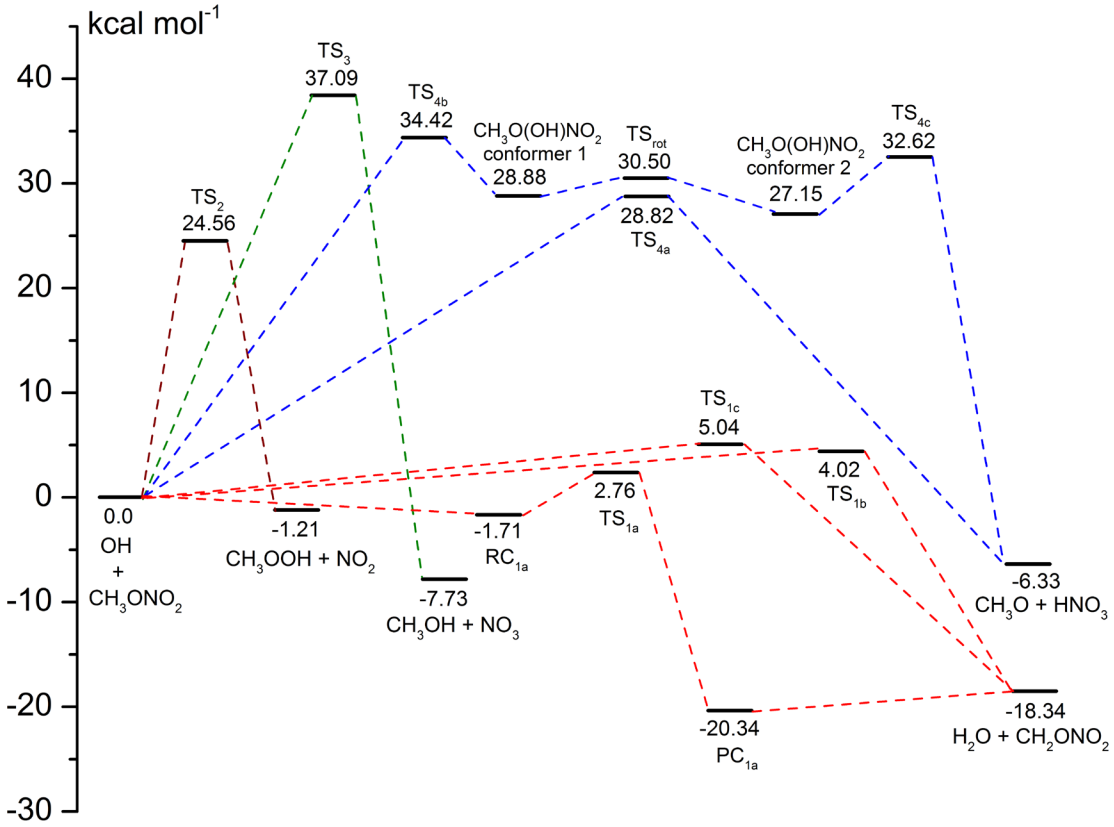

Figure 4. V_{MEP}, ΔZPE and V_a^G curves of the M06-2X/6-31+G** level (top) and the F12ave/CBSave//M06-2X level (bottom) for the out-of-plane OH + CH_3ONO_2 → H_2O + CH_2ONO_2 channel via TS_{1a}. The higher level (HL) V_{MEP} and V_a^G curves (bottom) were obtained by using the HL energies of the reactants, RC_{1a}, TS_{1a}, PC_{1a} and products, with more HL IRC points calculated by the expression devised by us previously (see text).[49]

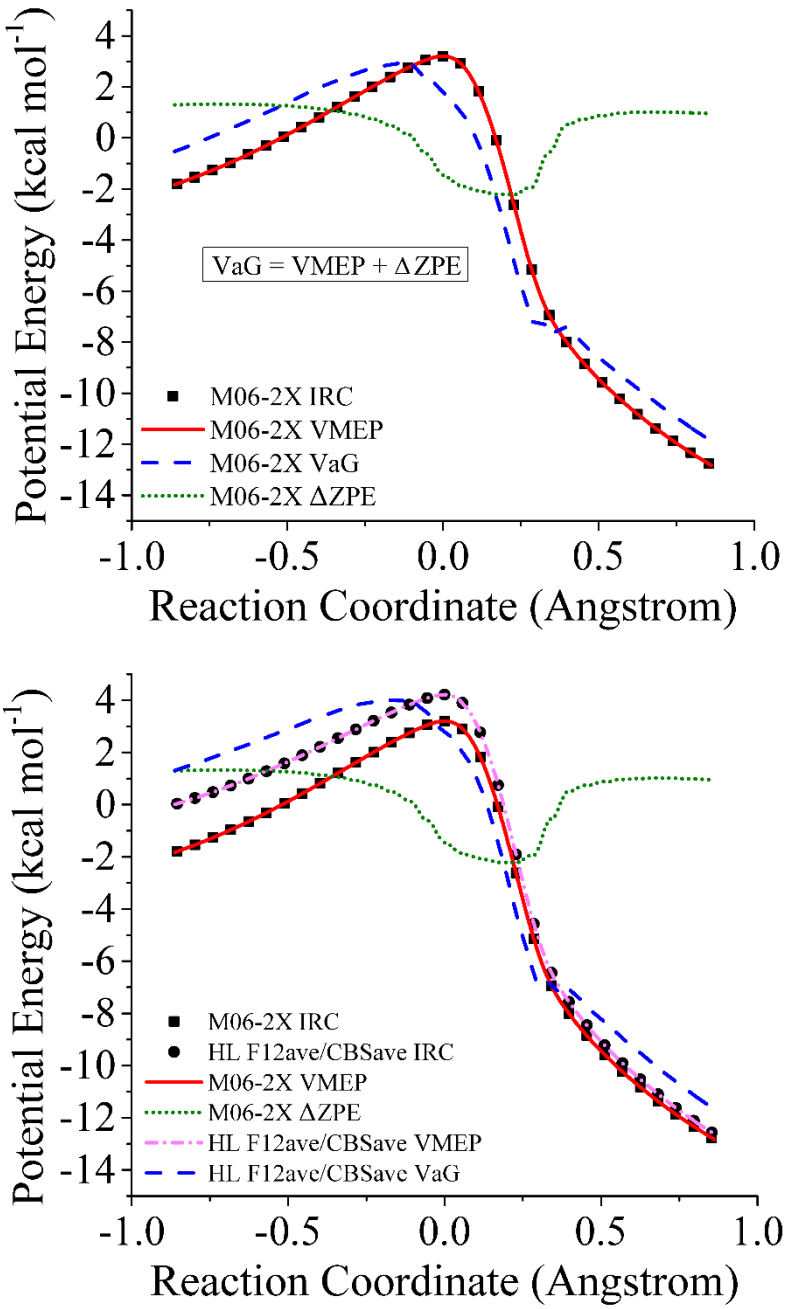

Figure 5. Computed rate coefficients (k; in cm^3 $molecule^{-1}$ s^{-1}) for the OH + CH_3ONO_2 → H_2O + CH_2ONO_2 reaction (channel 1(a)) at different temperatures (T) obtained at different VTST levels using the M06-2X/6-31+G** IRC (computed k values have been multiplied by two to account for two out-of-plane H abstraction sites with hydrogen bond-like interaction).

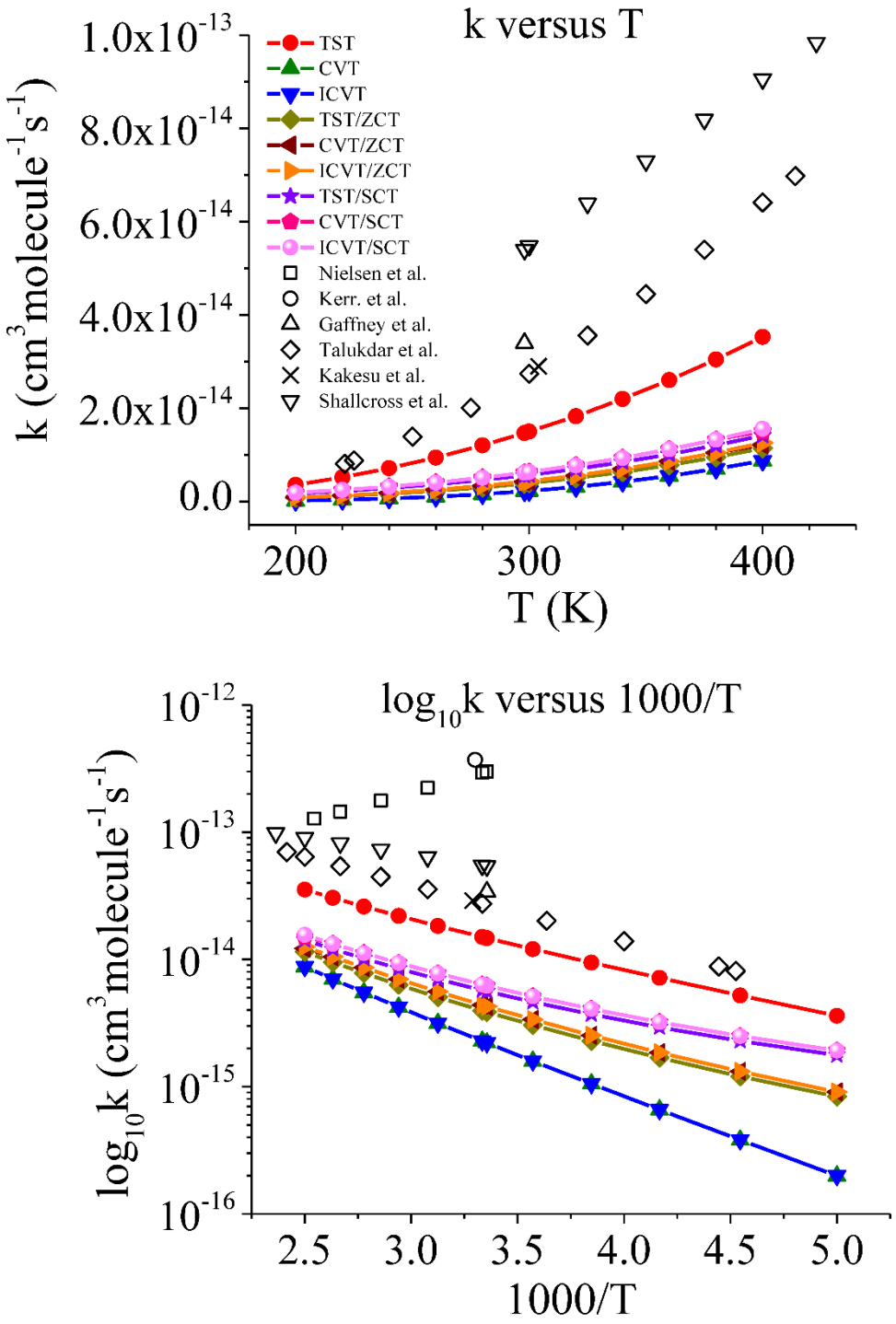

Figure 6. Rate coefficients (k; in cm^3 $molecule^{-1}$ s^{-1}) computed at different VTST levels for the OH + CH_3ONO_2 → H_2O + CH_2ONO_2 reaction (reaction 1(a)) with the HL F12ave/CBSave//M06-2X/6-31+G** IRC in the temperature range between 200 K and 400 K (computed k values have been multiplied by two to account for two H abstraction sites with hydrogen bond).

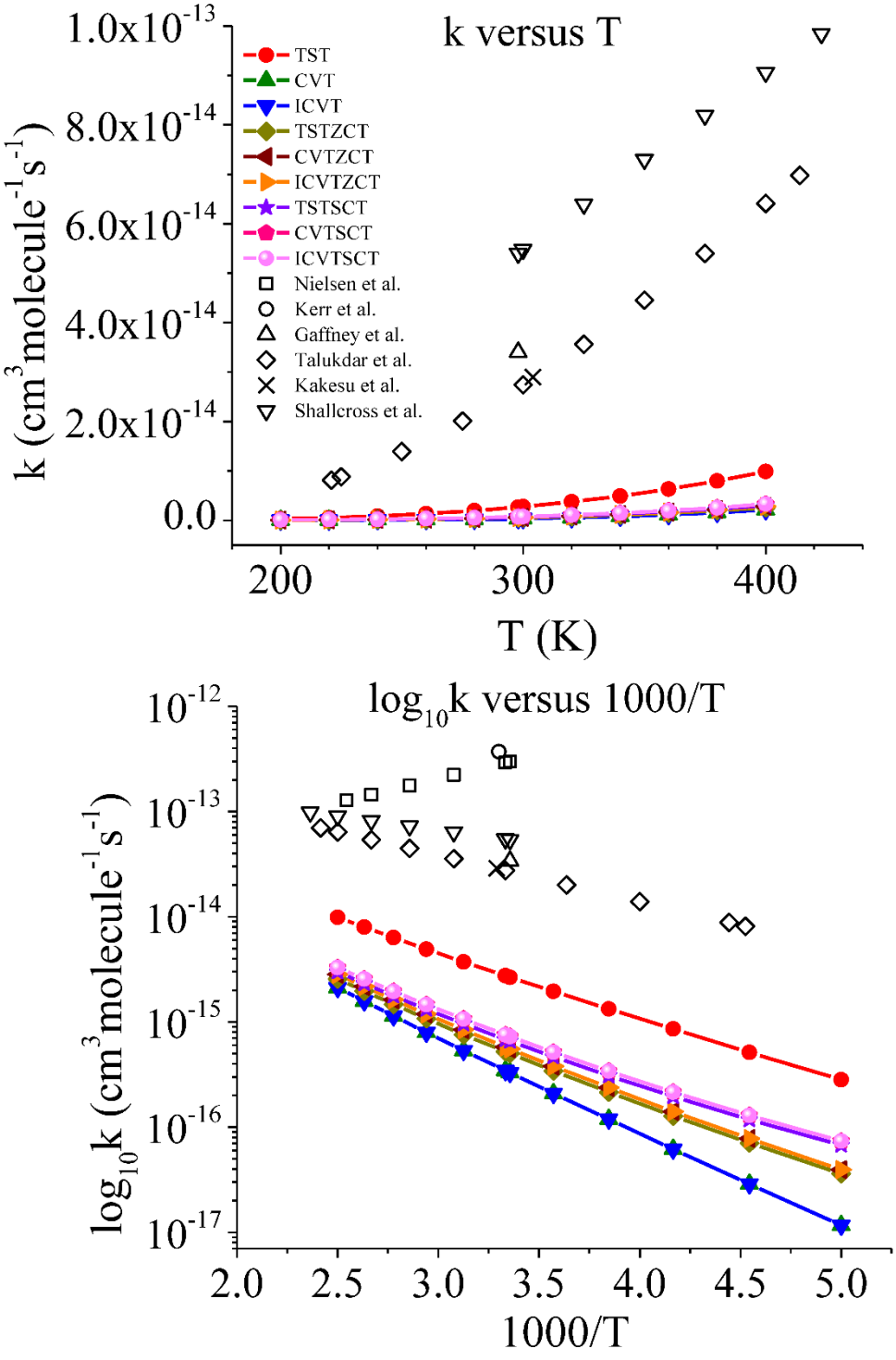

Figure 7. Computed ICVT/SCT rate coefficients (k; in cm^3 $molecule^{-1}$ s^{-1}) of reactions (1a), (1b) and (1c), as well as the total rate coefficients of the $OH + CH_3ONO_2 \rightarrow H_2O + CH_2ONO_2$ reaction with the HL F12ave/CBSave//M06-2X/6-31+G** IRC in the temperature range between 200 K and 400 K {k(total) = 2k(1a) + 2k(1b) + k(1c)}.

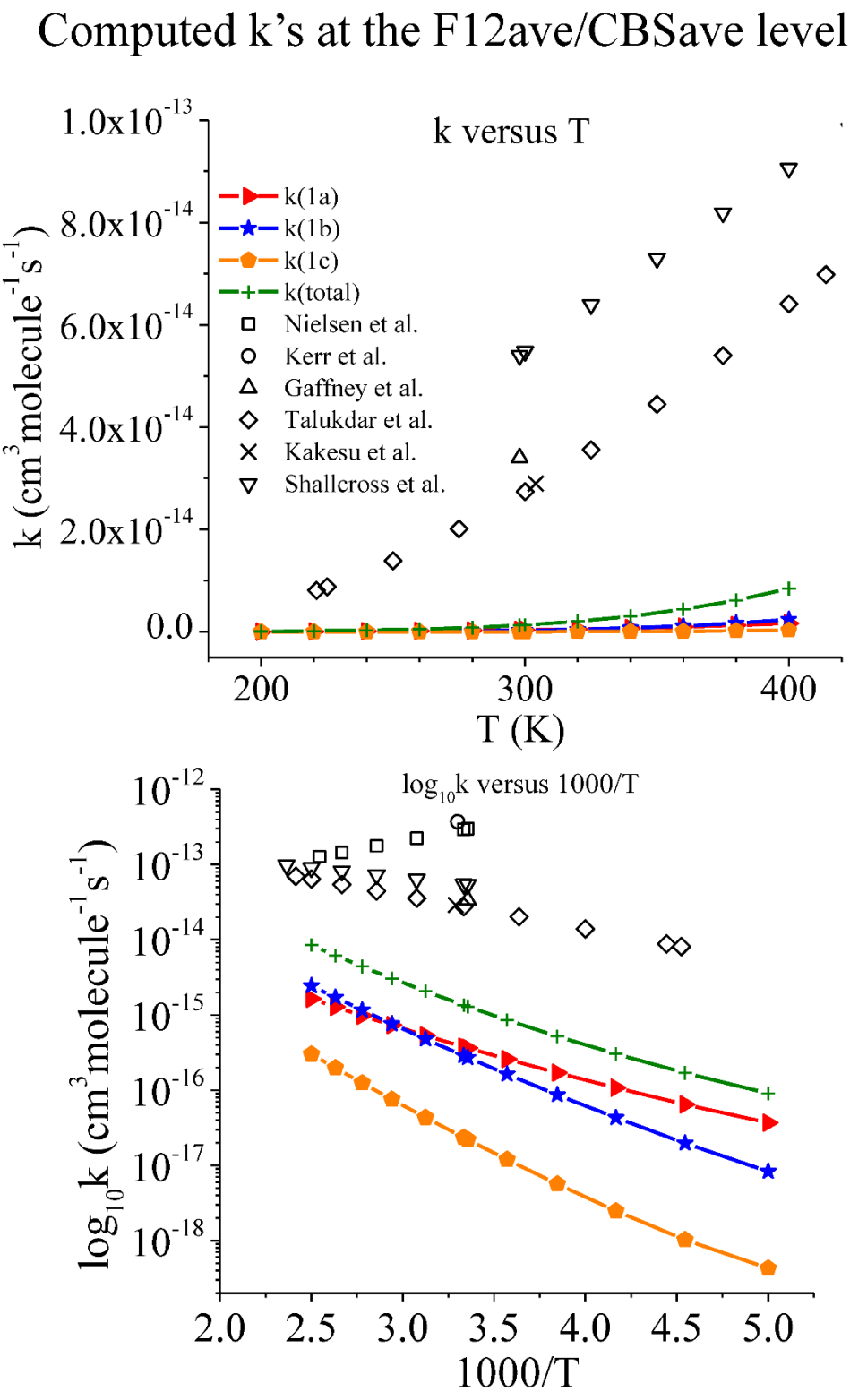

Figure 8 Computed ICVT/SCT rate coefficients (k; in cm^3 $molecule^{-1}$ s^{-1}) of reactions (1a), (1b) and (1c), as well as the total rate coefficients of the $OH + CH_3ONO_2 \rightarrow H_2O + CH_2ONO_2$ reaction with the HL F12ave/CBSave//M06-2X/6-31+G** IRC in the temperature range between 200 K and 400 K {k(total) = 2k(1a) + 2k(1b) + k(1c)}, with the HL F12ave/CBSave//M06-2X/6-31+G** barrier heights for channels 1(a), 1(b) and 1(c) reduced by 2.5 $kcal.mol^{-1}$ (see text).

Computed k's at the F12ave/CBSave level

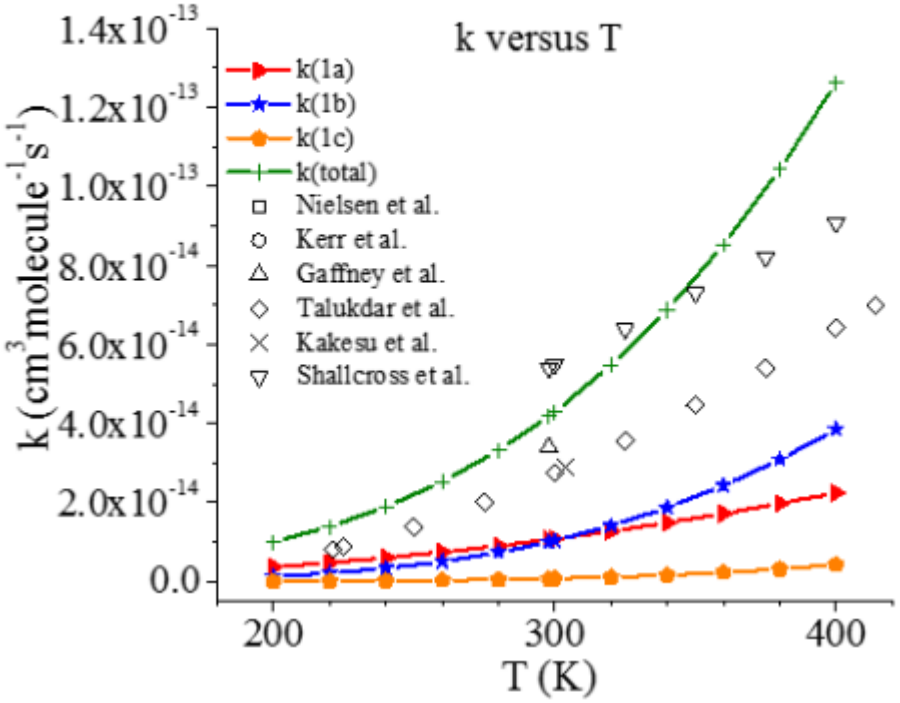

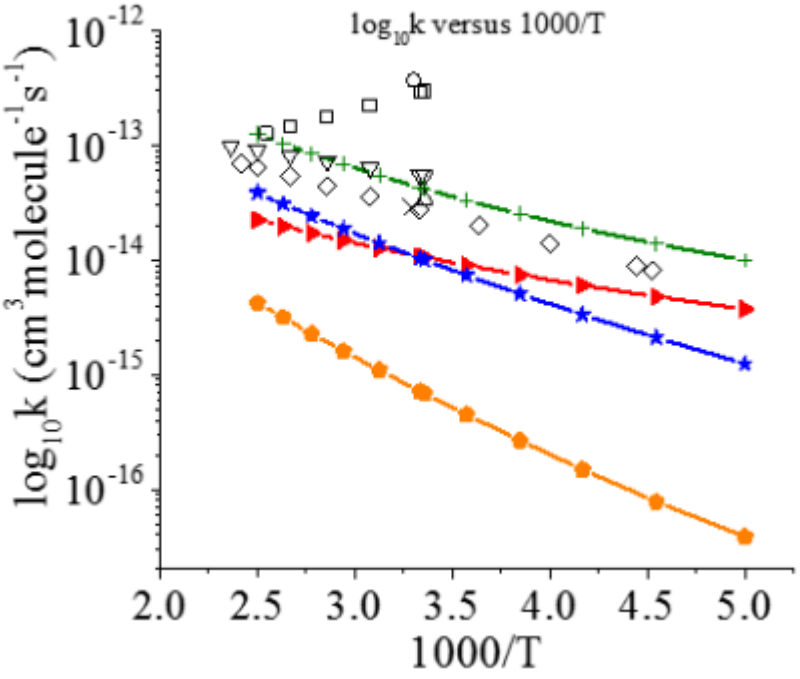

Supplementary Information

Contents

SI1.A note on calculation of improved single-level V_{MEP} curves

As noted in the "Theoretical considerations and computational details" section, improved single-level direct dynamics calculations (48) were carried out, with the M06-2X/6-31+G** V_{MEP} curve as the lower level (LL) and the higher-level (HL) V_{MEP} curve obtained by using the computed HL energies of five stationary points, namely, the separated reactants, RC, TS, PC and the separated products computed at the UCCSD(T*)-F12ave/CBSave level. More IRC points on the HL V_{MEP} were obtained by the scaling expression devised by us previously (equation (5),(49)). The HL V_{MEP} was used in the improved single-level direct dynamics calculations.

Also, improved single-level direct dynamics calculations were carried out with the interpolated single-point energies (VTST-ISPE) approach (48) at the UCCSD(T*)-F12ave/CBSave level, again with the M06-2X/6-31+G** level as the lower level (LL). The higher-level (HL) interpolated/extrapolated VTST-ISPE V_{MEP} curves were obtained by mapping with the computed HL energies of the five stationary points, namely, the separated reactants, RC, TS, PC and the separated products. However, the HL V_{MEP} curves obtained with these five

stationary points were unreasonable as the V_{MEP} maximum moved away from s = 0 (to s = -0.024 Å). This occurred also in our previous study on the Cl + CH_3ONO_2 reaction (11). Consequently, more IRC points were obtained by the scaling expression devised by us previously (equation (5),(49)), instead of performing extra HL single-point energy calculations on the LL IRC points, because it was found in our previous study that the HL V_{MEP} curves obtained with HL IRC energies have their maxima away from s = 0 (11).

SI2.

NO_2 formation: OH + CH_3ONO_2 → CH_3OOH + NO_2 --- Channel (2)

The geometry of the TS in channel (2′), TS_2, optimized at the M06-2X/6-31+G** level is shown in Figure 1. The computed imaginary vibrational frequency of TS_2, 988i cm^{-1}, corresponds to the asymmetric O…O…N stretching mode, indicating that TS_2 undergoes O-N bond breaking and O-O bond formation via a S_N2 mechanism to release NO_2, when the O atom of the OH radical attacks the O atom next to the methyl group. In TS_2, the breaking C-N bond is elongated by 33% while the forming O-O bond is longer than that in CH_3OOH by 22%. Hence, it is not obvious whether TS_2 is reactant-like or product-like, as the elongations of the breaking C-N bond and the forming O-O bond are comparable. The computed reaction energies (ΔE_e^{RX}) and activation energies ($\Delta E_e^{\ddagger}$) of channel (2) at various levels of theory are summarized in Table 1. The best computed ΔE_e values (labelled as F12ave/CBSave) were obtained by averaging the four CBS values {*i.e.* the UCCSD(T*)-F12a/CBS1, UCCSD(T*)-F12b/CBS1, UCCSD(T*)-F12a/CBS2 and UCCSD(T*)-F12b/CBS2 values}. The best computed ΔE_e^{RX} and $\Delta E_e^{\ddagger}$ values are -1.72 ± 0.01 and 24.08 ± 0.17 kcal mol^{-1}. It should be noted that the uncertainty in the computed $\Delta E_e^{\ddagger}$ value is much larger than that in the computed ΔE_e^{RX} value by a factor of seventeen. The best computed ΔE_e^{RX} and $\Delta E_e^{\ddagger}$ values are smaller than the corresponding M06-2X values by 2.00 and 5.78 kcal mol^{-1} respectively. The large discrepancy in $\Delta E_e^{\ddagger}$ between the M06-2X and the F12ave/CBSave levels indicates a poor performance by the M06-2X functional in predicting the barrier height in this channel. The best computed ΔH_{298K}^{RX} of -1.16 kcal mol^{-1} agrees fairly with the value of -2.96 kcal mol^{-1} determined using the available heats of formation ($\Delta H_{f,298K}$) of CH_3ONO_2 (50), OH (51), CH_3OOH (52) and NO_2 (51,53) as the difference between these reaction enthalpies is 1.8 kcal mol^{-1}. This discrepancy is reduced to 1.25 kcal mol^{-1} when our previously computed $\Delta H_{f,298K}$ value, -29.71 kcal mol^{-1} (11), was used for CH_3ONO_2 instead of the value from the tabulation

of Burcat et al. (50). Including the zero-point energy (ZPE) correction and the spin-orbit correction for OH, the best computed ΔE_{0K}^{RX} and $\Delta E_{0K}^{\ddagger}$ values of -1.21 and 24.56 kcal mol^{-1} are obtained. This indicates that channel (2) has a high activation barrier and, therefore, its contribution to the total rate coefficient of the OH + CH_3ONO_2 reaction is negligible.

SI3

NO_3 formation: OH + CH_3ONO_2 → CH_3OH + NO_3 --- Channel (3)

The geometry of the TS in channel (3′), TS_3, optimized at the M06-2X/6-31+G** level is shown in Figure 1. The imaginary vibrational frequency of 1251i cm^{-1} corresponds to the asymmetric O…C…O stretching mode, which shows that TS_3 undergoes O-C bond breaking and C-O bond forming via a S_N2 mechanism to release NO_3 when the O atom in the OH radical attacks the C atom in the methyl group. The breaking O-C bond in TS_3 is elongated by 29% while the forming C-O bond is longer than the equilibrium value of 1.41 Å in CH_3OH by 25%, and so the TS_3 is not reactant-like or product-like. The computed ΔE_e^{RX} and $\Delta E_e^{\ddagger}$ values at various levels of theory are summarized in Table 2. The best computed ΔE_e^{RX} and $\Delta E_e^{\ddagger}$ values at the F12ave/CBSave level are -7.99 ± 0.12 and 36.07 ± 0.11 kcal mol^{-1} respectively, which are smaller than the corresponding M06-2X values by 5.78 and 1.64 kcal mol^{-1} respectively. Although the $\Delta E_e^{\ddagger}$ value computed with the M06-2X functional shows better agreement with the F12ave/CBSave value than was the case for channel (2), there is a large discrepancy in the ΔE_e^{RX} computed values at the M06-2X/6-31+G** and the F12ave/CBSave levels, indicating that the ΔE_e^{RX} computed with the M06-2X functional is unreliable for the overall reaction enthalpy for this channel. It is surprising that the best computed ΔH_{298K}^{RX} value of -8.01 kcal mol^{-1} is more positive than the value of -11.77 kcal mol^{-1} determined from the available $\Delta H_{f,298K}$ values of CH_3ONO_2 (50), OH (51), CH_3OH (62-67) and NO_3 (68) by 3.76 kcal mol^{-1}. This difference is still more than 3 kcal mol^{-1} even when our previously computed $\Delta H_{f,298K}$ of CH_3ONO_2 (11) is used instead of the value from the tabulation of Burcat *et al.* (50). The significant energy difference probably comes from the $\Delta H_{f,298K}$ value of CH_3OH $\{\Delta H_{f,298K}(CH_3OH)\}$ used in the evaluation of ΔH_{298K}^{RX}. First, it is noted the $\Delta H_{f,298K}(CH_3OH)$ of –(49.0 ± 3.0) kcal mol^{-1} in ref.(50) is obtained by averaging the nine values in the literature (54-59), which were derived from the corresponding standard enthalpies of formation of the liquid ($\Delta H_{f,liquid}$) and the standard enthalpies of vaporization (ΔH_{vap}) determined decades ago. Also, the nine literature values, ranging from -51.1 kcal mol^{-1} to -47.94 kcal mol^{-1}, have a large

spread of 3 kcal mol^{-1}. The above two points cast doubt on the reliability of the $\Delta H_{f,298K}(CH_3OH)$. As a result, it was calculated in the present study by considering the following reaction.

$$CH_3OH \rightarrow CO + 2H_2 \qquad \text{----------(6)}$$

With a highly reliable $\Delta H_{f,298K}(CO)$ value of -26.417 ± 0.041 kcal mol^{-1} from CODATA (61) and $\Delta H_{f,298K}(H_2)$ = 0 kcal mol^{-1} by definition, $\Delta H_{f,298K}(CH_3OH)$ can be determined from the computed ΔH_{298K}^{RX} of the above reaction. F12 calculations were carried out on CO and H_2 at the experimental r_e values (69) of 1.128323 and 0.74144 Å, respectively, to obtain ΔE_e^{RX}. ZPEs of CO and H_2 were evaluated using the experimental vibrational frequencies (69) of 2169.81 and 4401.213 cm^{-1} respectively, while the ZPE of CH_3OH was calculated from the computed M06-2X vibrational frequencies. The vibrational thermal correction at 298 K (ΔE_v^{298K}) is dominated by the vibrational thermal contribution of CH_3OH as those of CO and H_2 are nearly zero due to their large vibrational frequencies. The ΔE_e^{RX}, ΔE_{0K}^{RX} and ΔH_{298K}^{RX} of the $CH_3OH \rightarrow CO + 2H_2$ reaction, as well as the determined $\Delta H_{f,298K}(CH_3OH)$ and the available literature values for $\Delta H_{f,298K}(CH_3OH)$, are summarized in Table 3. Our re-evaluated $\Delta H_{f,298K}(CH_3OH)$ is -47.61 kcal mol^{-1}, which is higher than the highest literature value of -47.94 kcal mol^{-1} by 0.33 kcal mol^{-1}. When this derived $\Delta H_{f,298K}(CH_3OH)$ of -47.61 kcal mol^{-1} and $\Delta H_{f,298K}(CH_3ONO_2)$ of -29.71 kcal mol^{-1} are used, the ΔH_{298K}^{RX} of channel (3) becomes -9.83 kcal mol^{-1}. The difference between the determined ΔH_{298K}^{RX} and our computed ΔH_{298K}^{RX} is thus greatly reduced to 1.82 kcal mol^{-1}, which is comparable to the corresponding difference of 1.8 kcal mol^{-1} for channel (2) (see previous section). Therefore the $\Delta H_{f,298K}(CH_3OH)$ value of -47.61 kcal mol^{-1} is recommended over the nine literature values used in ref.(50). The best computed ΔE_{0K}^{RX} and $\Delta E_{0K}^{\ddagger}$ values at the F12ave/CBSave level are -7.73 and 37.09 kcal mol^{-1} respectively. Although the computed ΔH_{298K}^{RX} value of -8.01 kcal mol^{-1} indicates that channel (3) is exothermic, the large reaction barrier height of 37.09 kcal mol^{-1} means that this reaction will only make an extremely small contribution to the overall $OH + CH_3ONO_2$ rate coefficient. As a result, channel (3) was also not considered in the rate coefficient calculations.

SI4

HNO_3 formation: OH + CH_3ONO_2 → CH_3O + HNO_3 --- Channel (4)

The reaction leading to HNO_3 formation can take place through a concerted mechanism, in which the reactants proceed to the products via a transition state, or through a stepwise mechanism involving adduct formation (see equation 4′). Regarding the concerted mechanism, the located transition state, TS_{4a} shown in Figure 1, has an imaginary vibrational frequency of 772i cm^{-1} which corresponds to the asymmetric O…N…O stretching mode. This shows that TS_{4a} undergoes O-N bond breaking and N-O bond forming via a S_N2 mechanism to give CH_3O and HNO_3 when the O atom in the OH radical attacks the N atom in CH_3ONO_2. Both the breaking O-N bond and the forming N-O bond are elongated by ~30% and so TS_{4a} is neither reactant-like nor product-like. The computed ΔE_e^{RX} and $\Delta E_e^{\ddagger}$ values at the different levels of theory used are summarized in Table 4. The best computed ΔE_e^{RX}, $\Delta E_e^{\ddagger}$ and ΔH_{298K}^{RX} values, at the F12ave/CBSave level, are -6.58 ± 0.03, 27.29 ± 0.17 and -6.78 kcal mol^{-1} respectively. Our best computed ΔH_{298K}^{RX} agrees with the value of -7.77 kcal mol^{-1} determined from the available $\Delta H_{f,298K}$ values of CH_3ONO_2 (50), OH (51), CH_3O (70) and HNO_3 (68) to within 1 kcal mol^{-1}, and better agreement is achieved when our previously computed $\Delta H_{f,298K}$ of CH_3ONO_2 (11) is used. The concerted reaction via TS_{4a} is expected to have a small rate coefficient because of its high barrier of 28.82 kcal mol^{-1}. Concerning the stepwise mechanism, CH_3ONO_2 can undergo OH addition via TS_{4b} to form an adduct labelled as "$CH_3O(OH)NO_2$ conformer 1", which could then undergo rotation about the O-N bond to give a more stable conformer labelled as "$CH_3O(OH)NO_2$ conformer 2". Conformer 2 finally dissociates into CH_3O and HNO_3 via TS_{4c} (see equation 4′ above). The M06-2X geometries of the two adduct conformers are given in Figure 2 and their energies as well as those of the rotational TS (TS_{rot}), relative to the separate reactants, are given in Table 5. The OH group in conformer 2 lies in the plane of the C, O and N atoms while the OH group in conformer 1 does not lie in this plane. At the highest F12ave/CBSave level, conformer 2 is more stable than conformer 1 by 1.73 kcal mol^{-1} and the rotational barrier from conformer 1 to conformer 2 is 1.62 kcal mol^{-1} (including ZPE and OH spin-orbit corrections). Conformer 2 will then dissociate to CH_3O and HNO_3 via TS_{4c} with a barrier of 5.47 kcal mol^{-1}. In spite of the low rotational barrier, it is unlikely that the separate reactants proceed to conformer 2 as they have to overcome a large barrier of 34.42 kcal mol^{-1}, corresponding to TS_{4b}, to form conformer 1. This channel, involving HNO_3 formation, is not expected to contribute to the overall reaction rate coefficient.

SI5.Table SI1. $k^{ICVT/SCT}$ values obtained with the HL UCCSD(T*)-F12ave/CBSave//M06-2X IRC for $2k_{1a}$, $2k_{1b}$ and k_{1c} from barrier heights ($\Delta E_e^{\ddagger}$) of 4.22, 5.72 and 7.25 kcal mol^{-1} respectively.

T (K)	$2k_{1a}$	$2k_{1b}$	k_{1c}	$k_{total} = 2k_{1a} + 2k_{1b} + k_{1c}$
200	7.37E-17	1.66E-17	4.27E-19	9.07E-17
220	1.29E-16	3.93E-17	1.03E-18	1.70E-16
221				
225				
240	2.15E-16	8.60E-17	2.48E-18	3.04E-16
250				
260	3.41E-16	1.74E-16	5.64E-18	5.20E-16
275				
280	5.17E-16	3.26E-16	1.19E-17	8.55E-16
290				
298	7.28E-16	5.43E-16	2.20E-17	1.29E-15
300	7.55E-16	5.74E-16	2.35E-17	1.35E-15
303				
304				
320	1.07E-15	9.56E-16	4.32E-17	2.06E-15
325				
340	1.45E-15	1.62E-15	7.52E-17	3.06E-15
350				
358				
360	1.95E-15	2.32E-15	1.24E-16	4.40E-15
375				
380	2.56E-15	3.42E-15	1.97E-16	6.17E-15
393				
400	3.28E-15	4.89E-15	3.01E-16	8.47E-15
414				
423				

SI6.Table SI2. $k^{ICVT/SCT}$ values obtained with the HL UCCSD(T*)-F12ave/CBSave//M06-2X IRC for $2k_{1a}$, $2k_{1b}$ and k_{1c} from barrier heights ($\Delta E_e^{\ddagger}$) of 1.72, 3.22 and 4.75 kcal mol^{-1} respectively. $\Delta E_e^{\ddagger}$ values for 1a, 1b and 1c are reduced by 2.5 $kcal.mol^{-1}$ from those used in SI5 (see text).

T (K)	$2k_{1a}$	$2k_{1b}$	k_{1c}	$k_{total} = 2k_{1a} + 2k_{1b} + k_{1c}$
200	7.45E-15	2.49E-15	3.87E-17	9.98E-15
220	9.57E-15	4.19E-15	7.81E-17	1.38E-14
221				
225				
240	1.20E-14	6.67E-15	1.49E-16	1.88E-14
250				
260	1.48E-14	1.01E-14	2.66E-16	2.52E-14
275				
280	1.80E-14	1.47E-14	4.50E-16	3.32E-14
290				
298	2.12E-14	2.00E-14	6.86E-16	4.19E-14
300	2.15E-14	2.07E-14	7.17E-16	4.29E-14
303				
304				
320	2.54E-14	2.82E-14	1.09E-15	5.47E-14
325				
340	2.97E-14	3.74E-14	1.61E-15	6.87E-14
350				
358				
360	3.44E-14	4.85E-14	2.28E-15	8.52E-14
375				
380	3.94E-14	6.17E-14	3.14E-15	1.04E-13
393				
400	4.49E-14	7.71E-14	4.23E-15	1.26E-13
414				
423				